Mössbauer Spectroscopy of the Spin Coupled Fe^{2+}−{FeNO}^{7} Centers of Nitrosyl Derivatives of Deoxy Hemerythrin and Density Functional Theory of the {FeNO}^{7}($S = {}^3/_2$) Motif

Jorge H. Rodriguez,*,[1] Yao-M. Xia, and Peter G. Debrunner

Contribution from the Department of Physics, University of Illinois at Urbana-Champaign, Urbana, Illinois 61801

Received January 13, 1999

Abstract: The mixed-valence diiron centers of nitrosyl derivatives of deoxy hemerythrin have been studied by variable-temperature variable-field Mössbauer spectroscopy. The adduct formed by the reaction of deoxy hemerythrin (deoxyHr) with nitric oxide (deoxyHrNO) produced spectra consistent with a binuclear center of the form $Fe^{2+}(S_1 = 2)$−{FeNO}$^7(S_2 = {}^3/_2)$ where the two iron species are antiferromagnetically coupled. We have analyzed spectra within the framework of the spin Hamiltonian $H = J\mathbf{S}_1\bullet\mathbf{S}_2 + \sum_{i=1}^{2} = \{\mathbf{S}_i\bullet\tilde{\mathrm{D}}_i\bullet\mathbf{S}_i + \beta\mathbf{S}_i\bullet\tilde{g}_i\bullet\mathbf{H} + \mathbf{S}_i\bullet\tilde{a}_i\bullet\mathbf{I}_i + \mathbf{I}_i\bullet\tilde{P}_i\bullet\mathbf{I}_i - \beta_n g_n\mathbf{H}\bullet\mathbf{I}_i\}$ that includes exchange, zero-field splitting, electronic Zeeman, magnetic hyperfine, electric quadrupole, and nuclear Zeeman interactions, respectively. We have obtained the following parameters that reproduce simultaneously Mössbauer spectra and EPR g values: $J = 27.8$ cm^{-1}, $D_1 = +5.96$ cm^{-1}, $E_1 = +0.18$ cm^{-1}, $D_2 = +18.93$ cm^{-1}, $E_2 = +2.65$ cm^{-1}, $\tilde{a}_1/g_n\beta_n = -(18.5,10.4,13.8)$ T, $\tilde{a}_2/g_n\beta_n = -(29.7,25.0,\sim 22)$ T, $R(\tilde{a}_1 \rightarrow \tilde{P}_1) = (18,12,67)°$, $R(\tilde{a}_2 \rightarrow \tilde{P}_2) = (55,53,29)°$ and $R(\tilde{D}_1 \rightarrow \tilde{D}_2) = (0,90,28)°$. In addition, at 100 K, we determined the isomer shifts (δ_{Fe}) 1.21 and 0.68 mm/s and quadrupole splittings (ΔE_Q) +2.66 and +0.61 mm/s for the Fe^{2+} and {FeNO}^{7} sites, respectively. We have also analyzed spectra with the $S^{eff} = {}^1/_2$ Hamiltonian for the ground state $H^{eff} = \beta\mathbf{S}^{eff}\bullet\tilde{g}^{eff}\bullet\mathbf{H} + \sum_{i=1}^{2}\{\mathbf{S}^{eff}\bullet\tilde{A}_i^{eff}\bullet\mathbf{I}_i + \mathbf{I}_i\bullet\tilde{P}_i\bullet\mathbf{I}_i - \beta_n g_n\mathbf{H}\bullet\mathbf{I}_i\}$ and have obtained parameters in the effective spin representation. In addition, we discuss the spectra of a second adduct of deoxyHr obtained by its reaction with NO in the presence of fluoride (deoxyHrFNO) which exhibits similar, but not equal, parameters to those of deoxyHrNO. Contrary to the parent form (deoxyHr) where the two ferrous ions are Mössbauer equivalent, the nitrosyl adducts have two iron sites which produce distinctly different spectra and have quite different magnetic and electronic properties. The isomer shifts of the {FeNO}^{7} sites are significantly reduced with respect to the high-spin ferrous configuration and enhanced with respect to the high-spin ferric configuration. To elucidate the physical origin of Mössbauer parameters from {FeNO}^{7}($S = {}^3/_2$) sites we have applied Kohn−Sham density functional theory to the representative complex $Fe(C_9H_{21}N_3)(NO)(N_3)_2$ [Pohl and Wieghardt, *J. Chem. Soc., Dalton Trans.* **1987**, 187]. The unusual isomer shifts have been traced to strong valence electron delocalization within the {FeNO}^{7} unit, whereby some electrons are almost equally shared by metal (i.e., d_{xz}, and d_{yz}) and NO π^* orbitals.

1. Introduction

Hemerythrin (Hr) is an oxygen-transporting non-heme protein found in marine invertebrates.[2−6] It can be considered the prototype and best characterized of a class of diiron proteins that interact with dioxygen. Hemerythrin has the physiologically important forms deoxyHr and oxyHr which contain pairs of high spin ferrous (Figure 1) and high-spin ferric ions, respectively. While the diferrous form appears to require a μ-hydroxo bridge, there is experimental evidence (e.g., ^{1}H NMR isotropic shifts) for a μ-oxo diferric core.[2,3] The proposed mechanism for reversible binding of dioxygen by hemerythrin can be represented by the reaction[2−7] shown in Scheme 1 where the proton from the hydroxo bridge is shuttled to the peroxide upon binding of O_2.

It is known, mostly from magnetic susceptibility and Mössbauer spectroscopy,[8,9] that the pairs of irons in deoxyHr and oxyHr are antiferromagnetically coupled and have diamagnetic ground states. The strength of the coupling between two weakly interacting iron sites can be quantified by the exchange constant of the Heisenberg Hamiltonian given by eq 1. The lower values

$$H_{ex} = J\mathbf{S}_1\bullet\mathbf{S}_2 \tag{1}$$

of J estimated for deoxyHr[10,11] with respect to oxyHr are consistent with their proposed hydroxo- and oxo-bridging schemes, respectively.

(1) Present address: Department of Chemistry, University of California at Berkeley, Berkeley, CA 94720-1460.

(2) Kurtz, D. M. *Chem. Rev.* **1990**, *90*, 585.

(3) Que, L., Jr.; True, A. E. *Prog. Inorg. Chem.* **1990**, *38*, 97.

(4) Stenkamp, R. E. *Chem. Rev.* **1994**, *94*, 715.

(5) Feig, A. L.; Lippard, S. J. *Chem. Rev.* **1994**, *94*, 759.

(6) Kurtz, D. M. *JBIC* **1997**, *2*, 159.

(7) Stenkamp, R. E.; Sieker, L. C.; Jensen, L. H. *J. Am. Chem. Soc.* **1984**, *106*, 618.

(8) Okamura, M. Y.; Klotz, I. M.; Johnson, C. E.; Winter, M.; Williams, R. J. P. *Biochemistry* **1969**, *8*, 1951.

(9) Garbett, K.; Johnson, C. E.; Klotz, I. M.; Okamura, M. Y.; Williams, R. J. P. *Arch. Biochem. Biophys.* **1971**, *142*, 574.

(10) The $H_{ex} = J\mathbf{S}_1\mathbf{S}_2$ representation of the Heisenberg Hamiltonian is not universal. All of the results given in this work are expressed in terms of this representation (i.e., eq 1). Other notations include: $H_{ex} = -J\mathbf{S}_1\mathbf{S}_2$, and $H_{ex} = -2J\mathbf{S}_1\mathbf{S}_2$.

(11) The values of J estimated from susceptibility experiments for deoxyHr and oxyHr are on the order of 30 and 144 cm^{-1}, respectively.[22,110]

10.1021/ja990129c CCC: $18.00
Published on Web 08/17/1999

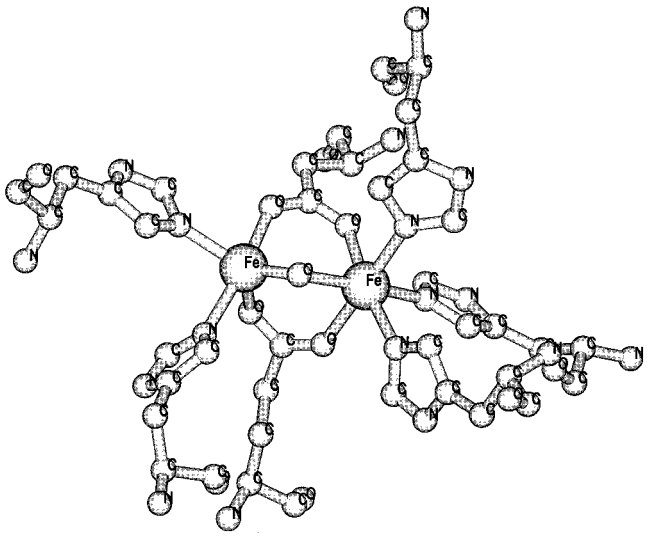

Figure 1. The diiron center of deoxyHr. The positional parameters correspond to the crystallographic structures of Stenkamp et al.[7,14]

Scheme 1

$$[Fe^{2+}(\mu\text{-}OH^{-})Fe^{2+}] + O_2 \rightleftharpoons [Fe^{3+}(\mu\text{-}O^{2-})Fe^{3+}OOH^{-}]$$

deoxyHr oxyHr

From the perspective of resonance spectroscopy techniques such as Mössbauer, EPR, and ENDOR, the diferrous and diferric cores of hemerythrin can provide relatively limited or no information due to the diamagnetism of their spin ground states. Among these techniques, however, Mössbauer spectroscopy is unique in its ability to probe both, diferric and diferrous, diamagnetic cores providing parameters such as isomer shifts (δ_{Fe}), quadrupole splittings (ΔE_Q), and asymmetry parameters (η). Mixed valent cores of diiron proteins often have half integer spin ground states (i.e., Kramers doublets) which greatly enhance the possibilities of resonance techniques. Spectra of mixed valence centers can provide significant information related to the exchange, zero-field splitting, and magnetic hyperfine interactions affecting their individual iron sites. Therefore, it is of great interest to apply Mössbauer spectroscopy to the study of mixed-valence cores of hemerythrin, such as those of its nitric oxide adducts, to gain insight about their various electric and magnetic interactions. From a mechanistic perspective it is also of interest to study the nitric oxide adducts of hemerythrin since these have been proposed as analogues of a possible semi-metHr superoxide intermediate in the oxygenation reaction.[3,12]

The Parent Form: DeoxyHr. Various forms of hemerythrin have been crystallographically characterized.[7,13−17] The structure of the diferrous form (deoxyHr) initially known to 2 Å resolution[14] has been further refined.[17] As shown in Figure 1, deoxyHr has five- and six-coordinate iron ions bridged by a μ-hydroxo (proton not shown))[6,18] and by two carboxylato groups, one each from aspartate and glutamate. The other terminal ligation sites are bound to nitrogens from imidazole side chains of five histidines.[4,14]

Previous Mössbauer measurements of deoxyHr yielded (around 77 K) a single doublet with isomer shift and quadrupole splitting values of 1.19 mm/s and 2.81 mm/s,[8,9,19] respectively, characteristic of high-spin ferrous ions.[20] The equivalent quadrupole doublets of the two iron sites should arise from dominant valence contributions to their electric field gradients (characteristic of high-spin ferrous ions) that preclude observation of minor lattice contributions which should be different for the five- and six-coordinate sites. DeoxyHr is EPR silent due to its singlet ground state.[21] The exchange interaction in deoxyHr is relatively weak with a coupling constant J estimated on the order of[10] 30 cm^{-1} from Evans susceptibility measurements[22] and 24 to 76 cm^{-1} from magnetic circular dichroism.[18,23] Reem and Solomon[18] and also Sage and Debrunner[24] have pointed out the effect of the zero-field splittings (ZFS) which being comparable in magnitude to the exchange interaction strongly perturb its energy levels. Similar ZFS effects have been more recently shown for the mixed-valence binuclear metal centers of reduced uteroferrin[25] and related model compounds.[26]

The Nitrosyl Adducts: deoxyHrNO and deoxyHrFNO. It has been reported that some single anions bind to the five-coordinate iron site of deoxyHr.[18] Similarly, nitric oxide binds reversibly to one iron of deoxyHr forming the adduct deoxyHrNO.[12] An important structural characteristic of deoxyHrNO is its bent FeNO moiety with an estimated Fe−N−O angle of[21] 111°. Upon binding to one iron site of deoxyHr, nitric oxide forms a $\{FeNO\}^7(S = {}^3/_2)$ group[27] which in turn couples antiferromagnetically to the $Fe^{2+}(S = 2)$ site producing a molecular Kramers doublet ground state. Previous Mössbauer measurements confirm such spin configurations for the two sites of deoxyHrNO since its 100 K spectra clearly showed two distinct doublets with isomer shifts and quadrupole splittings[21] characteristic of $\{FeNO\}^7(S = {}^3/_2)$ and $Fe^{2+}(S = 2)$. In contrast to its parent form, which is EPR silent, deoxyHrNO displays the unusual EPR tensor[21] $\tilde{g}^{eff}$ = (1.84,1.84,2.77). Sage and Debrunner[24] have rationalized these g values by calculating the effect of the large ZFS on the energy levels of the exchange interaction as indicated in section 4.B. These authors estimated the exchange constant of deoxyHrNO on the order of 20 cm^{-1} which is on the lower range of values estimated for deoxyHr.[18,22,23] Reaction of deoxyHr with nitric oxide in the presence of fluoride forms the adduct deoxyHrFNO which displays similar, but not equal, Mössbauer and EPR spectra relative to deoxyHrNO. The fluoride adduct yielded the EPR tensor[21] $\tilde{g}^{eff}$ = (1.80,1.80,2.58) which has also been interpreted as arising from a Kramers doublet that results from spin coupling between $Fe^{2+}(S = 2)$ and $\{FeNO\}^7(S = {}^3/_2)$.

While Scheme 1 describes the initial and final stages of the reaction of hemerythrin with dioxygen, it does not give insight about the possible order and mechanisms by which the proton

(12) Nocek, J. K.; D. M. Kurtz, J.; Sage, J. T.; Debrunner, P. G.; Maroney, M. J.; Que, L., Jr. *J. Am. Chem. Soc*. **1985**, *107*, 3382.
(13) Sheriff, S.; Hendrickson, W. A.; Smith, J. L. *Life Chem. Rep. Suppl. Ser*. **1983**, *1*, 305.
(14) Stenkamp, R. E.; Sieker, L. C.; Jensen, L. H.; McCallum, J. D.; Sanders-Loehr, J. *Proc. Natl. Acad. Sci. U.S.A*. **1985**, *82*, 713.
(15) Sheriff, S.; Hendrickson, W. A.; Smith, J. L. *J. Mol. Biol*. **1987**, *197*, 273.
(16) Holmes, M. A.; Stenkamp, R. E. *J. Mol. Biol*. **1991**, *220*, 723.
(17) Holmes, M. A.; Trong, I. L.; Turley, S.; Sieker, L. C.; Stenkamp, R. E. *J. Mol. Biol*. **1991**, *218*, 583.
(18) Reem, R. C.; Solomon, E. I. *J. Am. Chem. Soc*. **1987**, *109*, 1216.
(19) Spartalian, K. In *Applications of Mössbauer Spectroscopy*; Cohen, R. L., Ed.; Academic Press: New York, 1980; Vol. 2.
(20) Debrunner, P. G. In *Spectroscopic Approaches to Biomolecular Conformation*; Urry, D. W., Ed.; A. M. A. Press: Chicago, 1970; Chapter 6, pp 209−262.
(21) Nocek, J. K.; D. M. Kurtz, J.; Sage, J. T.; Debrunner, P. G.; Shiemke, A. K.; Sanders-Loehr, J.; Loehr, T: M. *Biochemistry* **1988**, *27*, 1014.
(22) Maroney, M. J.; Kurtz, D. M.; Noceck, J. M.; Pearce, L.; Que, L., Jr. *J. Am. Chem. Soc*. **1986**, *108*, 6871.
(23) Reem, R. C.; Solomon, E. I. *J. Am. Chem. Soc*. **1984**, *106*, 8323.
(24) Sage, J. T.; Debrunner, P. G. *Hyperfine Interact*. **1986**, *29*, 1399.
(25) Rodriguez, J. H.; Ok, H. N.; Xia; Y. M.; Debrunner, P. G.; Hinrichs, B. E.; Meyer, T.; Packard, N. *J. Phys. Chem*. **1996**, *100*, 6849.
(26) Rodriguez, J. H.; Xia, Y. M.; Debrunner, P. G.; Chaudhuri, P.; Wieghardt, K. *J. Am. Chem. Soc*. **1996**, *118*, 7542.
(27) We follow Enemark[32] in representing an iron nitrosyl complex with seven (Fe(d) plus NO π^*) electrons as $\{FeNO\}^7$. Similarly, $\{FeOO\}^8$ represents a complex with eight such electrons.

Scheme 2

$$[Fe^{2+}(\mu\text{-}OH^{-})Fe^{2+}] + O_2 \longrightarrow [Fe^{2+}(\mu\text{-}OH^{-})\{FeOO\}^{8}]$$

DeoxyHr — Proposed Intermediate

Scheme 3

$$[Fe^{2+}(\mu\text{-}OH^{-})Fe^{2+}] + NO \rightleftharpoons [Fe^{2+}(\mu\text{-}OH^{-})\{FeNO\}^{7}]$$

DeoxyHr — DeoxyHrNO

and electrons are transferred from the metal center to dioxygen. From the alternative mechanisms proposed,[3,14,28] Howard and Rees[28] considered two one-electron transfers bracketing proton transfer from the metal center to dioxygen. The initial reaction of this two-step process can be represented by Scheme 2 where $\{FeOO\}^8$ has the formal charge 2^+ and the terminal oxygen of superoxide is hydrogen bonded to the bridging ligand. It has been suggested[12] that the $\{FeOO\}^8$ unit has the limiting formulation $Fe^{3+}OO^-$. The notation of Scheme 2, although compatible, does not necessarily represent such ionic formulation.[27]

The reaction of deoxyHr with nitric oxide can be represented as shown in Scheme 3 where $\{FeNO\}^7$ has the formal charge 2^+, and according to Raman studies the terminal oxygen of the bound NO is involved in hydrogen bonding, a situation analogous to that of the proposed superoxide intermediate.[21,28] Therefore, it is of interest to elucidate the electronic structure responsible for the electric and magnetic interactions of deoxyHrNO since this can provide insight about similar interactions in a possible intermediate of the dioxygen binding reaction.

The Mössbauer parameters of $\{FeNO\}^7(S = {}^3/_2)$ complexes are of particular interest because these can not be adequately classified as arising from common idealized oxidation states of iron. In particular, their isomer shifts are reduced with respect to the high-spin ferrous and enhanced with respect to the high-spin ferric configurations. Several models for the electronic configuration of $\{FeNO\}^7$ complexes have been proposed.[29−34] However, some of these models have been described in terms of purely ionic electronic configurations of iron and NO and are inadequate for the interpretation of Mössbauer parameters which suggest considerable anisotropic covalency[35] and, in general, strong valence delocalization. The relatively recent development of nonlocal gradient-corrected exchange-correlation functionals[36−41] has made of Kohn−Sham[42] density functional theory (DFT)[43] a powerful method for the study of transition metal complexes. Self-consistent field DFT calculations can be performed to elucidate the electronic structure of metal complexes with open-shell configuration and can provide significant insight about their bonding and valence delocalization.

In this work we present a detailed spin Hamiltonian analysis of Mössbauer spectra of deoxyHrNO. The analysis of 4.2 K variable-field spectra was performed in the $(S_1 = 2) \times (S_2 = {}^3/_2)$ representation and yielded spin Hamiltonian parameters that reproduce simultaneously Mössbauer spectra and EPR g values. In particular, we have obtained values in the intrinsic spin representation for the isotropic exchange, zero-field splitting, and magnetic hyperfine interactions of the Fe^{2+} and $\{FeNO\}^7$ sites of deoxyHrNO. In addition, a $S^{eff} = {}^1/_2$ Hamiltonian has been used to determine effective parameters related to the Kramers doublet ground state. The substantial Mössbauer spectral changes of deoxyHrNO and deoxyHrFNO, with respect to deoxyHr, are discussed and related to the electronic configuration of their $\{FeNO\}^7$ sites. We present some semiquantitative arguments to interpret the magnitudes of isomer shifts, quadrupole splittings, and hyperfine tensors of $\{FeNO\}^7$ sites. In addition, we analyze zero-field variable-temperature spectra of deoxyHrFNO and the corresponding temperature dependence of its isomer shifts and electric field gradients. Finally, we present Kohn−Sham density functional theory calculations on the representative complex $FeL(NO)(N_3)_2$ ($L = C_9H_{21}N_3$)[44] to elucidate the correlation between valence electron delocalization and Mössbauer parameters of $\{FeNO\}^7(S = {}^3/_2)$ sites. The results from density functional theory are particularly important for the interpretation of Mössbauer results and are presented in section 5.

2. The Spin Hamiltonian

Intrinsic Spin Representation. The main interactions affecting the electronic and nuclear environments of a spin-coupled Fe^{2+}−$\{FeNO\}^7$ pair are given by the following spin Hamiltonian

$$H = H_{el} + H_{nu} \tag{2}$$

$$H_{el} = J\mathbf{S}_1\bullet\mathbf{S}_2 + \sum_{i=1}^{2}\{\mathbf{S}_i\bullet\tilde{D}_i\bullet\mathbf{S}_i + \beta\mathbf{S}_i\bullet\tilde{g}_i\bullet\mathbf{H}\} \tag{3}$$

$$H_{nu} = \sum_{i=1}^{2}\{\mathbf{S}_i\bullet\tilde{a}_i\bullet\mathbf{I}_i + \mathbf{I}_i\bullet\tilde{P}_i\bullet\mathbf{I}_i - \beta_n g_n\mathbf{H}\bullet\mathbf{I}_i\} \tag{4}$$

where the electronic Hamiltonian H_{el} includes isotropic exchange, zero-field splitting (ZFS), and electronic Zeeman interactions, in the intrinsic spin representation, of Fe^{2+} (site 1) and $\{FeNO\}^7$ (site 2), respectively. The nuclear Hamiltonian H_{nu} includes the magnetic hyperfine, electric quadrupole, and nuclear Zeeman interactions of both sites. We assume that the inequality $\langle H_{el}\rangle \gg \langle H_{nu}\rangle$ applies.

The leading term in eq 2 is the Heisenberg exchange Hamiltonian which has a number of eigenstates corresponding to the eigenvalues $S_1 - S_2$, ..., $S_1 + S_2$ of the total spin operator $\mathbf{S} = \mathbf{S}_1 + \mathbf{S}_2$. The energy corresponding to a given eigenstate of H_{ex} is

$$E(S) = {}^1/_2 J\{S(S+1) - S_1(S_1+1) - S_2(S_2+1)\} \tag{5}$$

The intrinsic tensors $\tilde{D}_i$ of eq 3 are chosen to be traceless, and the zero-field splittings can be expanded in terms of axial (D_i) and rhombic (E_i) parameters

(28) Howard, J. B.; Rees, D. C. *Adv. Protein Chem.* **1991**, *42*, 199.
(29) Wells, F. V.; McCann, S. W.; Wickman, H. H.; Kessel, S. L.; Hendrickson, D. N.; Feltham, R. D. *Inorg. Chem.* **1982**, *21*, 2306.
(30) Bill, E.; Bernhardt, F. H.; Trautwein, A. X.; Winkler, H. *Eur. J. Biochem.* **1985**, *147*, 177.
(31) Mingos, D. *Inorg. Chem.* **1973**, *12*, 1209.
(32) Enemark, J. H.; Feltham, R. D. *Coord. Chem. Rev.* **1974**, *13*, 339.
(33) Zhang, Y.; Pavlosky, A.; Brown, C. A.; Westre, T. E.; Hedman, B.; Hodgson, K. O.; Solomon, E. *I. J. Am. Chem. Soc.* **1992**, *114*, 9189.
(34) Brown, C. A.; Pavlosky, M. A.; Westre, T. E.; Zhang, Y.; Hedman, B.; Hodgson, K. O.; Solomon, E. I. *J. Am. Chem. Soc.* **1995**, *117*, 715.
(35) Orville, A. M.; Chen, V. J.; Kriauciunas, A.; Harpel, M. R.; Fox; B. G.; Münck, E: Lipscomb, J. D. *Biochemistry* **1992**, *31*, 4602.
(36) Becke, A. D. *Phys. Rev. A* **1988**, *38*, 3098.
(37) Becke, A. D. *J. Chem. Phys.* **1993**, *98*, 1372.
(38) Becke, A. D. *J. Chem. Phys.* **1993**, *98*, 5648.
(39) Lee, C.; Yang, W.; Parr, R. G. *Phys. Rev. B* **1988**, *37*, 785.
(40) Perdew, J. P. *Phys. Rev. B* **1986**, *33*, 8822.
(41) Perdew, J. P.; Wang, Y. *Phys. Rev. B* **1992**, *45*, 13244.
(42) Kohn, W.; Sham, L. J. *Phys. Rev.* **1965**, *140*, A1133.
(43) Parr, R. G.; Yang, W. *Density-Functional Theory of Atoms and Molecules*; Clarendon Press: Oxford, 1989.
(44) Pohl, K.; Wieghardt, K.; Nuber, B.; Weiss, J. *J. Chem. Soc.* **1987**, *Dalton Trans.*, 187.

$$H_{\mathrm{ZFS}} = \sum_{i=1}^{2}\{D_i[S_{zi}^2 - {}^1/_3 S_i(S_i+1)] + E_i(S_{xi}^2 - S_{yi}^2)\} \quad (6)$$

where the following relations hold

$$D_i = {}^3/_2 D_{zzi}$$

$$E_i = {}^1/_2(D_{xxi} - D_{yyi}) \quad (7)$$

The ZFS defines the axes system for each iron site. We have followed Blumberg[45] and used a proper coordinate system by letting z be the axis that makes D_i largest in magnitude and constraining D_i and E_i to have equal signs. This choice is consistent with the conditions $|D_{zz}| \geq |D_{yy}| \geq |D_{xx}|$, and $0 \leq {}^E/_D \leq {}^1/_3$.

The principal components of $\tilde{g}$ for Fe^{2+} have been found from the second-order expressions[46]

$$g_{xx} = g + \frac{2k}{\lambda}\left(E - \frac{D}{3}\right)$$

$$g_{yy} = g + \frac{2k}{\lambda}\left(-E - \frac{D}{3}\right)$$

$$g_{zz} = g + \frac{2k}{\lambda}\frac{2D}{3} \quad (8)$$

where we have used $g = {}^1/_3 \mathrm{Tr}\tilde{g}$, k is the orbital reduction factor, and λ is the spin−orbit coupling constant.

Effective Spin Representation. When the isotropic antiferromagnetic exchange is the dominant interaction in eq 3 the low temperature (e.g., $T \lesssim 4.2$ K) properties of a spin-coupled pair are mainly related to its ground (effective) spin manifold $S^{\mathrm{eff}} = S_1 - S_2$. More generally, for $kT \ll J(S^{\mathrm{eff}} + 1)$ only the ground state is significantly populated. In this case, it is possible and convenient to express the interactions of a spin-coupled pair in terms of the following effective spin Hamiltonian for the ground state:

$$H^{\mathrm{eff}} = \beta \boldsymbol{S}^{\mathrm{eff}} \bullet \tilde{g}^{\mathrm{eff}} \bullet \mathbf{H} + \sum_{i=1}^{2}\{S^{\mathrm{eff}} \bullet \tilde{A}_i^{\mathrm{eff}} \bullet \mathbf{I}_i + \mathbf{I}_i \bullet \tilde{P}_i \bullet \mathbf{I}_i - \beta_n g_n \mathbf{H} \bullet \mathbf{I}_i\} \quad (9)$$

where $\tilde{g}^{\mathrm{eff}}$ and $\tilde{A}^{\mathrm{eff}}$ are tensors, in the effective spin representation, corresponding to electronic Zeeman and magnetic hyperfine interactions, respectively. For the analysis of an Fe^{2+}−{FeNO}^{7} pair a term $\boldsymbol{S}^{\mathrm{eff}} \bullet \tilde{D}^{\mathrm{eff}} \bullet \boldsymbol{S}^{\mathrm{eff}}$ in eq 9 is omitted since the ZFS can not remove the degeneracy of the $S^{\mathrm{eff}} = {}^1/_2$ Kramers doublet. The effective spin representation is convenient for correlating EPR/ENDOR observables that arise from Kramers doublet ground states with Mössbauer parameters.

Our interpretation of Mössbauer spectra and EPR g^{eff} tensors of the binuclear iron centers rests on the determination of the intrinsic parameters of eq 2 and, in addition, on the effective parameters of eq 9 as described in section 3.[25,26]

Electric Quadrupole Interaction. The nuclear excited-state quadrupole moment interacts with the electric field gradient (EFG) giving rise to an electric quadrupole interaction. There are two main sources of electric field gradient. First, there is a valence contribution which arises from the nonspherical valence charge of d electrons. Second, there is a contribution which originates in noncubic charge distributions from the lattice about the ion. Both sources of EFG are affected by distortions of core electrons which reduce the valence contribution and enhance the lattice effect. Sternheimer shielding factors can be introduced to account for these latter effects.[47] In addition, anisotropic covalency can introduce a third contribution to the EFG.[48] For a single electron, the three diagonal components of the traceless cartesian EFG tensor $\tilde{V}$ are given, in its principal axes, by

$$V_{ii} = {}^2/_7 e(1 - \mathrm{R})\langle r^{-3}\rangle \langle {L_i}^2 - 2\rangle \quad (10)$$

where $i = (x, y, z)$, $(1 - R)$ is the Sternheimer factor and $\langle r^{-3}\rangle$ is the mean value of r^{-3} for 3d electrons.[25,49] The parameter representing a departure from axial symmetry is

$$\eta = \frac{V_{xx} - V_{yy}}{V_{zz}} \quad (11)$$

where $0 \leq \eta \leq 1$ with the convention that $|V_{zz}| \geq |V_{yy}| \geq |V_{xx}|$.

The electric quadrupole interaction for each iron site is given by

$$H_{\mathrm{E_Q}} = \frac{eQV_{zz}}{12}[3I_z^2 - I(I+1) + \eta(I_x^2 - I_y^2)] \quad (12)$$

where e is the charge of the proton and Q is the nuclear quadrupole moment.

The quadrupole interaction tensor $\tilde{P}$ of eq 4 can have different principal axes relative to those of the other interactions in eqs 3 and 4 due to lattice contributions to the EFG or from covalency that distorts the symmetry of the iron electron orbitals. To parameterize $\mathbf{I} \bullet \tilde{P} \bullet \mathbf{I}$ in its principal axes, the EFG tensor can be expressed as a second rank irreducible spherical tensor which transforms according to the representation D^2 of the rotation group:

$$\tilde{V}'_{2q} = \sum_p \tilde{V}_{2p} D^2_{pq}(\alpha\beta\gamma) \quad (13)$$

where $\tilde{V}'_{2q}$ is a component with respect to the primed axes, and α, β, and γ are Euler angles that rotate the unprimed axes into the primed axes.[50] If a component p is defined in the ion-fixed frame and a component q in the EFG frame, then eq 13 expresses how the components of the EFG tensor in its principal axes relate to its components in the ion-fixed frame if they are not coaxial.

3. Materials and Methods

Mössbauer Spectroscopy. The excitation beam for Mössbauer experiments originated in ^{57}Co sources of approximately 50 mCi activity diffused in rhodium. Doppler shifts of the incident γ beam were achieved by constant acceleration velocity transducers synchronized with a multichannel scaler which stored the count rate at 14.4 keV. The minimum line width at half maximum of the spectrometers was about 0.25 mm/s. The isolation, purification and preparation of samples of the parent form and nitrosyl derivatives have been reported in detail by Nocek et al.[21] Frozen solution samples of approximately 0.79 mM concentration were used for the Mössbauer experiments. The samples were not enriched with ^{57}Fe. This imposed relatively long acquisition times for recording Mössbauer spectra with a good signal to noise ratio. An analysis of spectra of deoxyHrNO in applied field at 4.2 K showed

(45) Blumberg, W. E. In *Magnetic Resonance in Biological Systems*; Ehrenberg, A., Malmström, B. G., Vangard, T., Eds.; Pergamon: Oxford, 1967.

(46) Abragam, A.; Bleaney, B. *Electron Paramagnetic Resonance of Transition Ions*; Dover: New York, 1986.

(47) Sternheimer, R. M. *Phys. Rev.* **1963**, *130*, 1423.

(48) Gütlich, P. In *Mössbauer Spectroscopy*; Gonser, U., Ed.; (Springer-Verlag: Berlin, Heidelberg, New York, 1975.

(49) Zimmermann, R. *Chem. Phys.* **1974**, *4*, 133.

(50) Brink, D. M.; Satchler, G. R. *Angular Momentum*; Clarendon Press: Oxford, 1968.

the presence of two iron impurity species. The impurities were identified as diferric ($\delta_{Fe} = 0.46$ mm/s and $\Delta E_Q = 1.18$ mm/s) and diferrous ($\delta_{Fe} = 1.10$ mm/s and $\Delta E_Q = 2.90$ mm/s) dimers which contribute 6 and 30% of the total area, respectively.

The analysis of Mössbauer spectra was carried out by searching in the multiparameter space of intrinsic (2) and effective (9) Hamiltonians with a genetic algorithm.[25,51−54] There were three main iterative steps:

(i) We simulated variable-field 4.2 K spectra by diagonalization of the $S^{eff} = {}^1/_2$ Hamiltonian and determined $\tilde{A}^{eff}_{1,2}$ and quadrupole interaction parameters (i.e., sign of ΔE_Q; η). The tensor $\tilde{g}^{eff}$ was known from EPR.[21]

(ii) We diagonalized the electronic Hamiltonian 3 and determined intrinsic parameters (J, D_i, E_i, g_i) that closely reproduced the EPR $\tilde{g}^{eff}$ tensor.[24]

(iii) We diagonalized and parameterized the intrinsic Hamiltonian 2. The electronic parameters determined in (ii) were part of an initial guess which also included the nuclear (a_i) parameters and relative orientations of the intrinsic tensors. The optimized parameters reproduced simultaneously applied-field Mössbauer spectra and $\tilde{g}^{eff}$ from EPR.

Density Functional Theory. The crystallographic structure of FeL-$(NO)(N_3)_2$[44] was used as the geometrical input. All electrons and all atoms were included in open-shell spin-unrestricted (U) self-consistent field (SCF) calculations. The use of a spin-unrestricted formalism permits the description of spin-polarized open-shell systems since α and β orbitals can have different spatial localizations.

Several combinations of exchange and correlation functionals were used. The results presented in this work are mainly from the combination of Becke[36] gradient-corrected exchange and Perdew−Wang[40,41] nonlocal correlation (BPW91). The former exchange functional was also used in conjunction with the nonlocal correlation of Lee−Yang−Parr[39] (BLYP) to perform analogous calculations. In addition, two hybrid methods were used. The three-parameter exchange of Becke[36−38,55] in conjunction with Lee−Yang−Parr[39] correlation (B3LYP). This constitutes a hybrid method that combines Hartree−Fock[56−59] with Slater[42,60,61] and gradient-corrected Becke[36−38] exchange functionals. Within the B3LYP method, the correlation is introduced by a combination of the local and nonlocal functionals of Vosko−Wilk−Nusair[55] and Lee−Yang−Parr,[39] respectively. The three-parameter exchange of Becke was also used with the correlation of Perdew−Wang (B3PW91).[40,41]

Single-point calculations used the all-electron triple-split-valence basis[59,62,63] 6-311G* for first row elements. For iron we used the all-electron basis optimized by Wachters[64] and Hay[65] by means of the scaling factors of Raghavachari and Trucks.[66]

Gaussian-94[67] was used to carry out the SCF calculations using a tight[68] convergence criterion. The wavefunctions were analyzed with MOLDEN[69] to obtain electronic density contours. Atomic charges, spin densities, and atomic orbital occupancies were calculated within the natural population analysis (NPA) framework developed by Weinhold et al.[70−73] Within this framework, the atom-centered basis set used to expand the unrestricted Kohn−Sham orbitals is transformed into a complete orthonormal set of natural localized atomic orbitals (NAO).[70−72] Calculations were carried out on the IBM-SP2 cluster of Mahui High Performance Computing Center (MHPCC), the IBM-SP2 and IBM-J40 parallel processing computers of the University of Illinois Research Computing Cluster (RCC), and the HP-Convex SPP-2000 cluster of the National Center for Supercomputer Applications (NCSA).

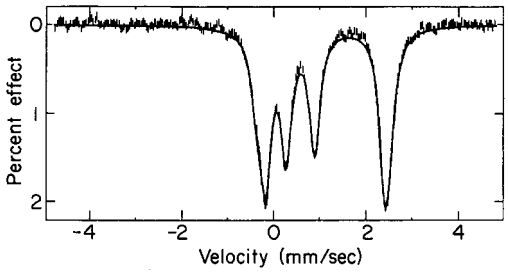

Figure 2. Spectrum of deoxyHrNO recorded at 100 K with no external field. Solid curve is an eight-line Lorentzian fit with the constraint of equal areas and equal widths for the two absorption lines of each doublet corresponding to Fe^{2+}, $\{FeNO\}^7$, and two unresolved impurity doublets characterized as diamagnetic Fe(II) ($\delta_{Fe} = 1.10$ mm/s, $\Delta E_Q = 2.90$ mm/s, 30% of area) and diamagnetic Fe(III) ($\delta_{Fe} = 0.46$ mm/s, $\Delta E_Q = 1.18$ mm/s, 6% of area). Inner and outer doublets correspond to $\{FeNO\}^7$ and Fe^{2+}, respectively. Parameters for the two sites of deoxyHrNO are given in Table 1.

4. Mössbauer Spectroscopy of Fe^{2+}−$\{FeNO\}^7$ Centers

Mössbauer measurements were performed under various conditions of temperature and applied magnetic field. We found important differences between spectra recorded in zero field at 4.2 K and those recorded at higher temperatures (i.e., $T \gtrsim 50$ K). Spectra recorded at 4.2 K without applied field (not shown) display relatively broad and featureless intensities corresponding to spontaneous magnetic hyperfine splitting. In contrast, high-temperature spectra of deoxyHrNO and deoxyHrFNO display two main and distinct quadrupole doublets corresponding to their Fe^{2+} and $\{FeNO\}^7$ sites. The $T \gtrsim 50$ K behavior results from fast spin−lattice relaxation rates. In the fast relaxation regime the magnetic hyperfine field is the thermal average of the fields produced by all accessible spin states and interacts with the nuclear spin to give characteristic high-temperature spectra. Figure 2 shows a 100 K spectrum of deoxyHrNO with no applied field which typifies fast relaxation. We now present Mössbauer results obtained under two experimental regimes.

(51) Holland, J. H. *Adaptation in Natural and Artificial Systems: An Introductory Analysis with Applications to Biology, Control, and Artificial Intelligence*; University of Michigan Press: Ann Arbor, MI, 1975.
(52) Goldberg, D. E. *Genetic Algorithms in Search, Optimization, and Machine Learning*; Addison Wesley: Reading, MA, 1989.
(53) Lucasius, C. B.; Kateman, G. *Chemom. Intell. Lab. Syst.* **1993**, *19*, 1.
(54) Forrest, S. *Science* **1993**, *261*, 872.
(55) Vosko, S. H.; Wilk, L.; Nusair, M. *Can. J. Phys.* **1980**, *58*, 1200.
(56) Hartree, D. R. *Proc. Cambridge Philos. Soc.* **1927**, *24*, 89.
(57) Fock, V. *Physik* **1930**, *61*, 126.
(58) Hartree, D. R. *The Calculation of Atomic Structure*; Wiley: New York, 1957.
(59) Hehre, W. J.; Radom, L.; Schleyer, P. v. R.; Pople, J. A. *Ab Initio Molecular Orbital Theory*; John Wiley & Sons: New York, 1986.
(60) Hohenberg, P.; Kohn, W. *Phys. Rev.* **1964**, *136*, B864.
(61) Slater, J. C. *Quantum Theory of Molecules and Solids. The Self-Consistent Field for Molecules and Solids*; McGraw-Hill: New York, 1974; Vol. 4.
(62) Krishnan, R.; Binkley, J. S.; Seeger, R.; Pople, J. A. *J. Chem. Phys.* **1980**, *72*, 650.
(63) Krishnan, R.; Frisch, M. J.; Pople, J. A. *J. Chem. Phys.* **1980**, *72*, 4244.
(64) Wachters, A. J. H. *J. Chem. Phys.* **1970**, *52*, 1033.
(65) Hay, P. J. *J. Chem. Phys.* **1977**, *66*, 4377.
(66) Raghavachari, K.; Trucks, G. W. *J. Chem. Phys.* **1989**, *91*, 1062.
(67) Gaussian 94, Revision E.2, Frisch, M. J.; Trucks, G. W.; Schlegel, H. B.; Gill, P. M. W.; Johnson, B. G.; Robb, M. A.; Cheeseman, J. R.; Keith, T.; Petersson, G. A.; Montgomery, J. A.; Raghavachari, K.; Al-Laham, M. A.; Zakrzewski, V. G.; Ortiz, J. V.; Foresman, J. B.; Cioslowski, J.; Stefanov, B. B.; Nanayakkara, A.; Challacombe, M.; Peng, C. Y.; Ayala, P. Y.; Chen, W.; Wong, M. W.; Andres, J. L.; Replogle, E. S.; Gomperts, R.; Martin, R. L.; Fox, D. J.; Binkley, J. S.; Defrees, D. J.; Baker, J.; Stewart, J. P.; Head-Gordon, M.; Gonzalez, C.; Pople, J. A. Gaussian, Inc.: Pittsburgh, PA, 1995.
(68) Frisch, M. J.; Frisch, A.; Foresman, J. B. *Gaussian 94 User's Manual*; Gaussian Inc.: Pittsburgh, 1995.
(69) Schaftenaar, G. MOLDEN, Molecular Density Package, CAOS/CAMM Center: Nijmegen, The Netherlands, 1991.
(70) Reed, A. E.; Weinhold, F. *J. Chem. Phys.* **1983**, *78*, 4066.
(71) Reed, A. E.; Weinstock, R. B.; Weinhold, F. *J. Chem. Phys.* **1985**, *83*, 735.
(72) Glendening, E. D.; Reed, A. E.; Carpenter, J. E.; Weinhold, F. *NBO 3.1*; Theoretical Chemistry Institute: University of Wisconsin, Madison, 1996.
(73) Glendening, E. D.; Badenhoop, J. K.; Reed, A. E.; Carpenter, J. E.; Weinhold, F. *NBO 4.0*; Theoretical Chemistry Institute: University of Wisconsin, Madison, 1996.

Table 1. Isomer Shifts and Quadrupole Splittings for DeoxyHrNO and DeoxyHrFNO

	T (K)	δ_{Fe}(mm/s)[a]	ΔE_Q(mm/s)
		deoxyHrNO	
Fe^{2+}	100	1.21	2.66
$\{FeNO\}^7$	100	0.68	0.61
		deoxyHrFNO	
Fe^{2+}	50	1.23[b]	3.13
	100		3.09
	150		3.04
	200		2.93
	250		2.77
$\{FeNO\}^7$	50	0.77	1.03[c]
	100	0.75	
	150	0.74	
	200	0.72	
	250	0.68	

[a] With respect to iron metal at room temperature. [b] The isomer shift of Fe^{2+} remains constant within this temperature range. [c] The quadrupole splitting of $\{FeNO\}^7$ remains constant within this temperature range.

4. A. High-Temperature Spectra. The parameters of Table 1 show that 50−250 K spectra of deoxyHrFNO produced an unusual combination of isomer shifts and quadrupole splittings that confirm the presence of $S_1 = 2$ and $S_2 = {}^3/_2$ iron species. Furthermore, these parameters display some temperature dependence. The results clearly show that as the temperature is lowered from 250 to 50 K, ΔE_Q of Fe^{2+} increases in absolute value by 0.36 mm/s, whereas ΔE_Q of $\{FeNO\}^7$ remains constant. A somewhat inverse trend is observed for the isomer shifts since, within the same temperature range, δ_{Fe} of $\{FeNO\}^7$ increases by 0.09 mm/s, whereas δ_{Fe} of Fe^{2+} remains constant.

Isomer Shifts. Table 1 shows nearly equal isomer shifts for the Fe^{2+} sites of deoxyHrNO ($\delta_{Fe} = 1.21$ mm/s) and deoxyHrFNO ($\delta_{Fe} = 1.23$ mm/s). These values are within the range expected for high-spin ferrous ions,[20,74,75] and their similarity suggests only minor geometrical differences between their first coordination spheres. We expect nearly equal s electron charge densities at the Fe^{2+} nuclei of deoxyHrNO and deoxyHrFNO which is in turn a sign of similar d electron populations. It follows that the presence of fluoride does not affect significantly the net charge densities of valence or inner s orbitals at the Fe^{2+} site of deoxyHrFNO. This observation suggests the absence of direct bonding between fluoride and the six-coordinate Fe^{2+} site in deoxyHrFNO.

There is some difference between the isomer shifts of the $\{FeNO\}^7$ sites of the two adducts. Fits with Lorentzian lines yielded, at 100 K, $\delta_{Fe} = 0.68$ mm/s for deoxyHrNO and $\delta_{Fe} = 0.75$ mm/s for deoxyHrFNO, in agreement with previous reports.[12,21,24,76] Nevertheless, both of these values are close to those reported for several quartet state monomeric $\{FeNO\}^7$ complexes as can be appreciated from Table 2. The somewhat higher value of δ_{Fe} for deoxyHrFNO relative to deoxyHrNO indicates that the presence of fluoride perturbs the valence electron density at its $\{FeNO\}^7$ site increasing the d electron shielding on s electrons. The variation of isomer shift for deoxyHrFNO is 0.09 mm/s over a temperature range of 200 K. Such temperature dependence can be explained by considering the extra contribution from the second-order Doppler shift which increases δ_{Fe} with decreasing temperature. Lang and Marshall[77] estimated the temperature-dependent isomer shift on the order of 6×10^{-4} mm/s-K, roughly of the magnitude measured for deoxyHrFNO.

Table 2. Mössbauer Parameters of Selected $\{FeNO\}^7$ ($S = {}^3/_2$) Complexes

T (K)	δ_{Fe}[a] (mm/s)	ΔE_Q (mm/s)	compd
4.2	0.66	−1.67	Fe(EDTA)(NO)[84]
4.2	0.66	−1.67	PC4,5O_2ase[84]
77	0.654	0.575[b]	Fe(5-C1-salen)(NO)[29]
4.2	0.62	1.31[b]	Fe(L)$(N_3)_2$(NO)[90]
4.2	0.68	−1.4	Putidamonooxin[30]
4.2	0.75	−1.0	IPNS-NO[35]
4.2	0.65	−1.2	IPNS-ACV-NO[35]

[a] With respect to iron metal at room temperature. [b] Sign of ΔE_Q not determined.

There is a large difference between the isomer shifts of Fe^{2+} and $\{FeNO\}^7$ sites in both nitrosyl adducts. The isomer shifts of the $\{FeNO\}^7$ sites are reduced with respect to typical values[76] measured for high-spin ferrous ions and enhanced with respect to values measured for high-spin ferric ions. This indicates that the irons within the $\{FeNO\}^7$ units have a different electronic configuration than either of these idealized configurations.

Electric Quadrupole Interaction. The quadrupole splittings measured at 100 K for the Fe^{2+} sites of deoxyHrNO (+2.66 mm/s) and deoxyHrFNO (+3.09 mm/s) correspond to a range expected for iron sites in distorted octahedral environments with nominal $d_{xy}^{\downarrow\uparrow}\, d_{xz}^{\uparrow}\, d_{yz}^{\uparrow}\, d_{x^2-y^2}^{\uparrow}\, d_{z^2}^{\uparrow}$ configuration, thus confirming their high-spin state. The signs of ΔE_Q for high-spin ferrous ions are closely related to the symmetry of their d orbital ground states and were obtained from simulations of spectra recorded in external fields. We follow the convention that the signs of ΔE_Q are given by the signs of V_{zz}. From Table S1 in the Supporting Information it follows that from the three (octahedral) t_{2g} orbitals only d_{xy} produces a positive expectation value $\langle V_{zz}\rangle$. Therefore, d_{xy} is identified as the orbital ground state which hosts two electrons. The larger magnitude of ΔE_Q for the fluoride adduct may reflect a stronger tetragonal compression at its ferrous site. Simulations in applied field also yielded the corresponding asymmetry parameters. For the Fe^{2+} site of deoxyHrNO we determined $0.23 \lesssim \eta \lesssim 0.29$. A preliminary analysis for deoxyHrFNO has given a small asymmetry parameter ($\eta \gtrsim 0$) which implies an EFG of axial symmetry.

The variation with temperature of the quadrupole splitting for the Fe^{2+} site of deoxyHrFNO is shown in Table 1. A temperature dependence is expected[78] for high-spin ferrous ions since the contributions to the EFG from d orbitals change with temperature, according to their Boltzmann populations. When orbital degeneracy is completely removed by the ligand field, at low temperatures, only the d orbital ground state is significantly occupied by the minority spin down (β) electron of the ferrous ion. In this case the contribution of the d orbital ground state to the EFG is maximum. At higher temperatures, higher lying d orbitals also become populated which reduces the valence EFG since their individual contributions, being proportional to $\langle L_i^2 - 2\rangle$ (Table S1), tend to cancel each other. An analysis of the temperature dependence of deoxyHrNO has not been performed but its behavior with temperature is expected to be similar to that of deoxyHrFNO.

In contrast to the large quadrupole splittings of the ferrous sites, the values measured at the same temperature for the $\{FeNO\}^7$ sites of deoxyHrNO (+0.61 mm/s) and deoxyHrFNO (+1.03 mm/s) are considerably smaller. As shown in Table 1,

(74) Greenwood, N. N.; Gibb, T. C. *Mössbauer Spectroscopy*; Chapman and Hall: London, 1971.
(75) Lang, G. *Q. Rev. Biophys.* **1970**, *3*, 1.
(76) Debrunner, P. G. *Hyperfine Interact.* **1990**, *53*, 21.
(77) Lang, G.; Marshall, W. *Proc. Phys. Soc.* **1966**, *87*, 3.
(78) Ingalls, R. *Phys. Rev.* **1964**, *133*, A787.

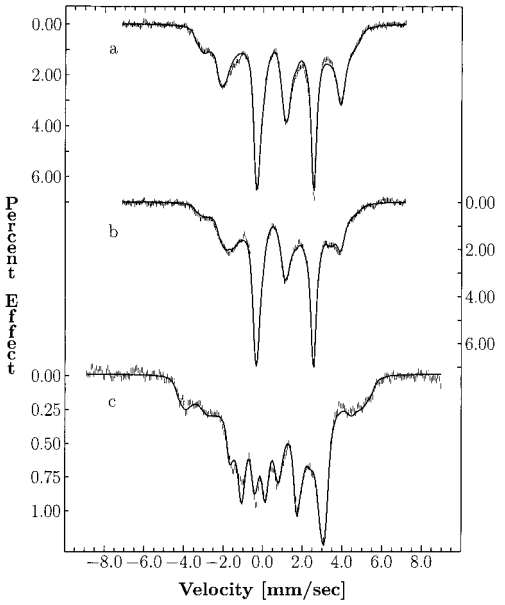

Figure 3. Spectra from sample of deoxyHrNO at 4.2 K recorded in applied fields of 0.032 T (a) parallel, (b) 0.032 T perpendicular, and (c) 4.9 T parallel with respect to the incident γ beam. Solid lines are simulations performed with the effective spin Hamiltonian (eq 9) and parameters given in Table 3. Simulations include two diamagnetic impurities with parameters given in text. Simulations performed with the intrinsic spin Hamiltonian (eq 2) (not shown) were of equivalent quality with parameters given in Table 4.

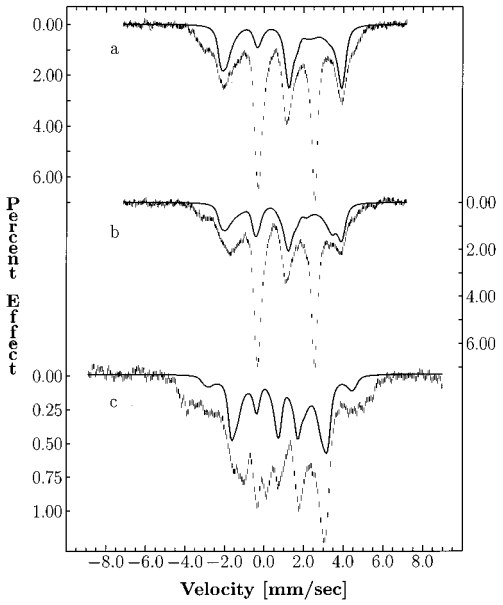

Figure 4. Contribution from Fe^{2+} site of deoxyHrNO to spectra recorded at 4.2 K in applied fields of (a) 0.032 T parallel, (b) 0.032 T perpendicular, and (c) 4.9 T parallel with respect to the incident γ beam. Solid lines are simulations performed with the effective spin Hamiltonian (eq 9) and parameters given in Table 3. Simulations performed with the intrinsic spin Hamiltonian (eq 2) (not shown) were of equivalent quality with parameters given in Table 4.

within a 50 to 250 K range, the quadrupole splitting of the $\{FeNO\}^7$ site of deoxyHrFNO shows no appreciable temperature dependence. A similar behavior is expected from deoxyHrNO. Thus, the temperature independence of the EFG for the $\{FeNO\}^7$ sites is also in contrast to the dependence exhibited by the ferrous sites.

4. B. Applied Field Spectra of DeoxyHrNO. Low-temperature spectra were recorded in applied fields to observe magnetic hyperfine interactions. Figure 3 shows the 4.2 K spectra obtained for deoxyHrNO in fields of 0.032 and 4.9 T. The corresponding simulations for the two magnetic sites are shown in Figures 4 and 5. Since we used samples of relatively low concentration, we do not expect significant effects from spin−spin relaxation. Also, since spin−lattice relaxation times become longer with decreasing temperature, we expected to reach a slow relaxation regime at 4.2 K. To verify these assumptions, Mössbauer data were taken at two different temperatures (i.e., 4.2 and 1.7 K) under the same applied field. Comparison of 4.2 and 1.7 K spectra showed no significant differences. This indicates that a slow electron spin relaxation regime has been reached at 4.2 K. Under these conditions the electron spin relaxation rate is slower than the nuclear precession frequency ($\sim 10^{-7}$ sec), and the nuclear spin can interact with a stationary hyperfine field. We now rationalize the spin Hamiltonian parameters determined by searching in the parameter space of eqs 2 and 9 following the procedures described in section 3.

Exchange Interaction and Zero-Field Splittings. The results for deoxyHrNO are presented in Table 4. Values for the exchange constant J, ZFS parameters D_i and E_i, and intrinsic $\tilde{g}_i$ tensors have been obtained for the Fe^{2+} and $\{FeNO\}^7$ sites by diagonalization of eq 3.

The net spin coupling has been interpreted in terms of Hamiltonian 1 where $S_1 = 2$ for Fe^{2+} and $S_2 = {}^3/_2$ for $\{FeNO\}^7$. According to the Anderson[79−81] model of superexchange, the magnitude and sign of the exchange constant results from

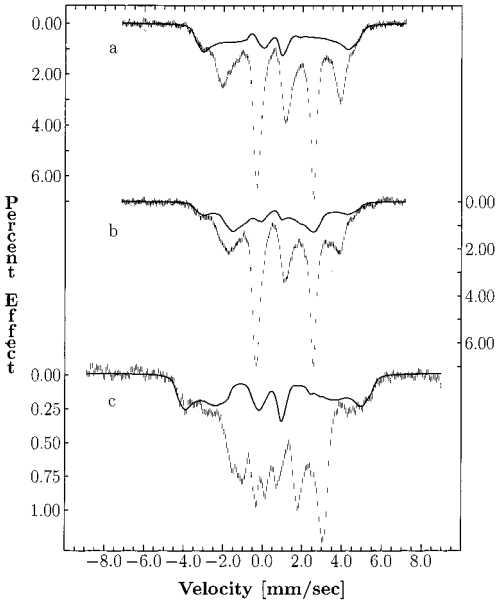

Figure 5. Contribution from $\{FeNO\}^7$ site of deoxyHrNO to spectra recorded at 4.2 K in applied fields of (a) 0.032 T parallel, (b) 0.032 T perpendicular, and (c) 4.9 T parallel with respect to the incident γ beam. Solid lines are simulations performed with the effective spin Hamiltonian (eq 9) and parameters given in Table 3. Simulations performed with the intrinsic spin Hamiltonian (eq 2) (not shown) were of equivalent quality with parameters given in Table 4.

competing ferromagnetic and antiferromagnetic contributions. When the former are dominant, J is negative, and when the latter are dominant, J is positive. The Mössbauer simulations

(79) Anderson, P. W. *Phys. Rev.* **1959**, *115*, 2.
(80) Anderson, P. W. In *Magnetism*; Rado, G. T., Suhl, H., Eds.; Academic Press: New York, 1963; Vol. 1.
(81) Hay, P. J.; Thibeault, J. C.; Hoffmann, R. J. *J. Am. Chem. Soc.* **1975**, *97*, 4884.

Table 3. Effective Hamiltonian Parameters for DeoxyHrNO

$S^{\text{eff}} = {}^1/_2$

$\tilde{g}^{\text{eff}}_{\text{EPR}} = (1.84,1.84,2.77)^a$

$\tilde{g}^{\text{eff}}_{\text{calc}} = (1.83,1.85,2.78)^b$

site	$\tilde{A}^{\text{eff}}/g_n\beta_n$ (T)	$R(\tilde{A}^{\text{eff}} \rightarrow \tilde{P})$ (deg)	$\Delta E_Q{}^c$ (mm/s)	η	$\delta_{Fe}{}^c$ (mm/s)	Γ (mm/s)
Fe^{2+}	−(24.9,16.3,31.5)	(72,85,14)	+2.66	0.23	1.21	0.31
{FeNO}^{7}	+(51.2,46.0,13.4)	(35,87,78)	+0.61	0.32	0.68	0.33

[a] Empirical tensor taken from Nocek et al.[21] [b] Tensor calculated from eq 3 with the intrinsic parameters of Table 4. [c] Isomer shifts and quadrupole splittings are values measured at 100 K.

Table 4. Intrinsic Hamiltonian Parameters for DeoxyHrNO

$J = 27.83\ \text{cm}^{-1}$

site	S	D^a (cm^{-1})	E (cm^{-1})	$\tilde{a}/g_n\beta_n$ (T)	$R(\tilde{a} \rightarrow \tilde{P})$ (deg)	$R(\tilde{a} \rightarrow \tilde{D}, \tilde{g})$ (deg)	$\tilde{g}^b$
Fe^{2+}	2	+5.96	+0.18	−(18.5,10.4,13.8)	(18,12,67)	(0, 0, 0)	(2.23,2.24,2.14)
{FeNO}^{7}	$^3/_2$	+18.93	+2.65	−(29.7,25.0,∼22)	(55,53,29)	(0,90,28)	(2.00,2.00,2.00)

[a] The principal axes of $\tilde{D}_2$ for {FeNO}^{7} in eq 2 are rotated with respect to those of $\tilde{D}_1$ according to $R(\tilde{D}_1 \rightarrow \tilde{D}_2) = (0,90,28)°$. The principal axes of $\tilde{D}_i$ and $\tilde{g}_i$ have been treated as coaxial. The principal axes of $\tilde{a}_1$ and $\tilde{a}_2$ were allowed to have different orientations; however, the simulations converged to a solution with coaxial hyperfine tensors. [b] The spin−orbit constant $\lambda = -103\ \text{cm}^{-1}$ and orbital reduction factor $k = 0.8$ were used to calculate the anisotropy of the ferrous $\tilde{g}_1$ tensor according to eq 8. The tensor $\tilde{g}_2$ was treated as isotropic with average value 2 as found for other iron nitrosyl complexes.[84]

for deoxyHrNO are consistent with a relatively weak antiferromagnetic coupling, and we have determined $J \approx +28\ \text{cm}^{-1}$. Within the field of molecular magnetism, the ability to determine exchange constants from analysis of Mössbauer spectra is fairly novel.[25]

The exchange interaction partially removes the original $(2S_1 + 1)(2S_2 + 1) = 20$ degeneracy and has states corresponding to the manifolds $S = {}^1/_2$, $^3/_2$, $^5/_2$, and $^7/_2$. It follows from eq 5 that the energies of the states of the total spin operator are given by

$$E(S) = {}^1/_2 J[S(S+1) - 39/4] \qquad (14)$$

The separation between the lower doublet and higher quartet is $^3/_2 J = 42\ \text{cm}^{-1}$. At the same time, the ZFS parameters for the two magnetic sites of deoxyHrNO are comparable in magnitude to the exchange constant as can be appreciated from the ratios $|J/D_1| \approx 4.66$ for Fe^{2+} and $|J/D_2| \approx 1.47$ for {FeNO}^{7} (Table 4). Clearly, H_{ZFS} strongly perturbs H_{ex} and mixes states from higher manifolds with the $S^{\text{eff}} = {}^1/_2$ ground state. Thus, the binuclear center is in an intermediate coupling regime where the condition $|J/D_i| \gtrsim 1$ applies.

The ZFS parameters are sensitive to asymmetries of the crystal field, in particular to distortions from a cubic arrangement of the surrounding ligands.[82] For instance, a crystalline field of axial symmetry, combined with spin−orbit coupling, can produce splittings between the intrinsic spin substates ($|M_{S_i}\rangle$) corresponding to differences in eigenvalues of the operator $D[S_{zi}^2 - {}^1/_3 S_i(S_i+1)]$.[82] The positive sign of D_1 indicates that $|M_{S_1} = 0\rangle$ is the ground state of the ferrous site. Similarly, the positive sign of D_2 implies that $|M_{S_2} = \pm {}^1/_2\rangle$ is the ground state for the {FeNO}^{7} site.[46,83]

The short Fe−NO bond (1.73 Å) introduces an axial compression in the distorted octahedral environment of the iron nitrosyl site. We also notice that calculated charge densities (section 5) for the mononuclear complex show that the nitrogen belonging to NO is nearly neutral in comparison to the other five nitrogens bound to iron which are fairly negative. For the {FeNO}^{7} site of deoxyHrNO the three oxygens bound to iron are expected to be more negative than the three bound nitrogens. Therefore, in deoxyHrNO the nitrogen belonging to NO should be substantially less negative than the other five atoms bound to iron. The axial parameter $D_2 = +18.9\ \text{cm}^{-1}$ is unusually large and should reflect not only the axially distorted ligand field but also the strong π delocalization which is particular to the Fe−NO bond. Previous Mössbauer analyses of mononuclear iron nitrosyl complexes have also determined rather large zero-field parameters.[35,84] We can compare the zero-field splittings of {FeNO}^{7} sites with other iron configurations as follows:

$$|D_{\{\text{FeNO}\}^7(S=3/2)}| \gtrsim |D_{\text{Fe}^{2+}(S=2)}| \gg |D_{\text{Fe}^{3+}(S=5/2)}| \gtrsim 0$$

The tensors corresponding to the various interactions in eq 2 do not, in general, share principal axes. Mössbauer spectra recorded in applied fields are particularly sensitive to differences in orientations of the ZFS, magnetic hyperfine and electric quadrupole interactions. The ZFS defines the axes system for each individual iron site and its orientation relative to other interactions, such as the electric quadrupole term, can be expressed in terms of Euler angles as illustrated by eq 13.

The relative orientations of the individual tensors are listed in Table 4. Figure 6 shows $\hat{o}_1(x_1, y_1, z_1)$ and $\hat{o}_2(x_2, y_2, z_2)$ which coincide with the principal axes of $\tilde{D}_1$ and $\tilde{D}_2$, respectively. Following the conventions of Brink and Satchler,[50] $R(\alpha = 0, \beta = 90, \gamma = 28)°$ first rotates (z_1, x_1) into $(z_2, -z_1)$, respectively, and subsequently $(-z_1, y_1)$ into (x_2, y_2). For the Fe^{2+} site the principal axes of $\tilde{D}_1$ and $\tilde{a}_1$ are coaxial whereas, for the iron site of {FeNO}^{7}, $\tilde{D}_2$ and $\tilde{a}_2$ do not share principal axes. The tensors $\tilde{a}_1$ and $\tilde{a}_2$ have the same orientation represented by $\hat{o}_1(x_1, y_1, z_1)$. Accordingly, the principal axes of the quadrupole interaction tensors $\tilde{P}_1$ and $\tilde{P}_2$ (not shown) are rotated with respect to $\hat{o}_1(x_1, y_1, z_1)$ by their respective Euler angles given in Table 4.

One important difference should be stated between the results obtained for deoxyHrNO and those of other mixed valent diiron proteins such as reduced uteroferrin[25] which has an Fe^{3+} $(S = {}^5/_2) - Fe^{2+}(S = 2)$ core. In uteroferrin the ZFS of the Fe^{2+} site dominates the perturbation on the states of the exchange Hamiltonian. This follows because for uteroferrin, which displays the ratio $|D_1/D_2| \approx 0.009$, the contribution from Fe^{3+}

(82) Bowers, K. D.; Owen, J. *Rep. Prog. Phys.* **1955**, *18*, 305.
(83) Gill, J. C.; Ivey, P. A. *J. Phys. C: Solid State Phys.* **1974**, *7*, 1536.
(84) Arciero, D. M.; Lipscomb, J. D.; Huynh, B. H.; Kent, T. A.; Münk, E. *J. Biol. Chem.* **1983**, *258*, 14981.

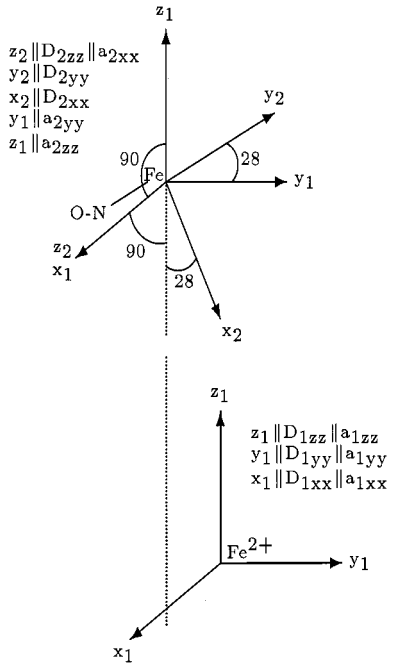

Figure 6. Relative tensor orientations of deoxyHrNO: The coordinate systems $\hat{o}_1(x_1, y_1, z_1)$ and $\hat{o}_2(x_2, y_2, z_2)$ are centered on Fe^{2+} and the iron site of {FeNO}^{7}, respectively, and correspond to the principal axes of $\tilde{D}_1$ and $\tilde{D}_2$. The Euler angles that relate $\hat{o}_1$ and $\hat{o}_2$ are shown. The dotted line (not drawn to scale) illustrates how the projection of the the origin of $\hat{o}_2$ falls on the (x_1, y_1) plane. The symbol || represents parallel axes. The z_2 axis is *approximately* parallel to the Fe−N(O) axis.

to the ZFS is negligible.[25] For this latter protein it was impossible to deduce the orientation of $\tilde{D}_1$, and the frames of $\tilde{D}_1$ and $\tilde{D}_2$ were treated as coaxial. By contrast, for deoxyHrNO, with a ratio $|D_1/D_2| \approx 0.32$, it was important to consider the relative orientation between the frames of $\tilde{D}_1$ and $\tilde{D}_2$.

Effective and Intrinsic Tensors. For conditions of strong coupling (i.e., $|J/D_i| \gg 1$) one can write explicit relations between the components of effective and intrinsic tensors. Assuming that these share principal axes, for $S_1 = 2$ and $S_2 = {}^3/_2$ we have[85−87]

$$\tilde{g}^{\text{eff}} = +2g_1 - g_2$$
$$\tilde{A}_1^{\text{eff}} = +2a_1$$
$$\tilde{A}_2^{\text{eff}} = -a_2 \qquad (15)$$

The ground-state tensor for deoxyHrNO, $\tilde{g}^{\text{eff}} = (1.84,1.84.2.77)$, has been measured by EPR.[21] As has been reported for deoxyHrNO,[21,24,76] uteroferrin,[24,25,88] and for the family of hemerythrins,[89] such unusual $\tilde{g}^{\text{eff}}$ tensors can not be adequately calculated from eqs 15. Instead, when the condition $|J/D_i| \gtrsim 1$ applies, one has to consider the mixing of the ground state with higher spin manifolds in order to account for the effects of ZFS.

Simulations of low field (e.g., 0.032 T) Mössbauer spectra with intrinsic (eq 2) and effective (eq 9) spin Hamiltonians are not very sensitive to small variations of $\tilde{g}_i$ or $\tilde{g}^{\text{eff}}$. The opposite is true for model calculations[24,88] which, by diagonalizing eq 3, can reproduce the empirical values of $\tilde{g}^{\text{eff}}$. During simulations of Mössbauer spectra in the intrinsic spin representation, knowledge of $\tilde{g}^{\text{eff}}$ from EPR constitutes an empirical constraint that imposes boundaries on the parameters acceptable as solutions to the electronic Hamiltonian 3. Consequently, we required that a single set of parameters reproduce simultaneously Mössbauer spectra (via eq 2) and $\tilde{g}^{\text{eff}}$ from EPR (via eq 3). The results presented in Table 3 show that empirical and calculated values for $\tilde{g}^{\text{eff}}$ are very close.

Effective hyperfine tensors were obtained from simulations based on eq 9 of the 4.2 K spectra shown in Figure 3. We notice that for higher fields (e.g., 4.9 T) the Zeeman splitting becomes more comparable to exchange and ZFS interactions and, consequently, $\tilde{A}_i^{\text{eff}}$ determined via eq 9 become an approximation. Accordingly, we have given greater weight to the low-field spectra during our optimization of $\tilde{A}_i^{\text{eff}}$. The intrinsic hyperfine tensors ($\tilde{a}_i$) were obtained from simulations of Mössbauer spectra (after substraction of impurities) based on eq 2 which can account for high-field Zeeman effects and also for large ZFS when $|J/D_i| \gtrsim 1$ applies. The results are presented in Tables 3 and 4. In the effective representation the ferrous tensor is very anisotropic with values $\tilde{A}_i^{\text{eff}}/g_n\beta_n = -(24.9,16.3,-31.5)$ T. We determined negative and positive signs for A_1^{eff} and A_2^{eff}, respectively, as predicted by eq 15. This fact provides further confirmation that {FeNO}^{7} has a spin lower than that of Fe^{2+}, consistent with $S_2 = {}^3/_2$. The negative or positive hyperfine signs imply that the internal field opposes or aids the applied field, respectively.

The intrinsic tensors are by themselves anisotropic. Analysis of spectra in the intrinsic representation yielded $(\tilde{a}_1/g_n\beta_n = -(18.5,10.4,13.8)$ T. The anisotropy of $\tilde{a}_1$ arises mostly from the orbital and traceless dipolar contributions to the hyperfine field. We notice that the ferrous tensor of deoxyHrNO shows some resemblance to that of the ferrous site of reduced uteroferrin $(\tilde{a}/g_n\beta_n = -(15.2,12.2,14.1)$ T).[25] The interpretation given for the hyperfine structure of Fe^{2+} in uteroferrin may also apply in the present case, namely that the parameters obtained are consistent with the presence of an orthorhombic environment at the ferrous site. However, in the present case the ratio $|E_1/D_1|$ is much smaller, and the rhombic contribution to the ZFS is less important.

For the {FeNO}^{7} site the analysis of spectra yielded $\tilde{A}_2^{\text{eff}}/g_n\beta_n = +(51.2,46.0,13.4)$ T in the effective representation and $\tilde{a}_2/g_n\beta_n = -(29.7,25.0,\approx 22.0)$ T in the intrinsic formalism. Therefore, the intrinsic tensor is by itself anisotropic. For this particular iron site the intrinsic simulations are very insensitive to the value of the z component. The value $a_{2zz} \approx -22.0$ T, although compatible with, is not determined by the simulations. Orville and Münck[35] also reported in their analysis of $S = {}^3/_2$ nitrosyl complexes of isopenicillin that, owing to their axial nature, the Mössbauer spectra of these complexes are relatively insensitive to the z component of the hyperfine tensor. The average value ${}^1/_3Tr\tilde{a}_2 \approx -26$ T can be compared with the value reported for the {FeNO}^{7}($S = {}^3/_2$) site of EDTA−Fe(II)−NO which was first studied by Arciero et al.[84] (${}^1/_3Tr\tilde{a}_2 \approx -23$ T) and later by Orville et al.[35] (${}^1/_3Tr\tilde{a}_2 \approx -26$ T). The latter value compares well with the value obtained here for deoxyHrNO. However, we notice that the spectral features of the isolated $S = {}^3/_2$ site of EDTA−Fe(II)−NO[84] are quite different from those of the spin coupled $S_2 = {}^3/_2$ site of deoxyHrNO.

(85) Scaringe, P. R.; Derek, J. H.; Hatfield, W. E. *Mol. Phys.* **1978**, *35*, 701.
(86) Bencini, A.; Gatteschi, D. *EPR of Exchange Coupled Systems*; Springer Verlag: Berlin, 1990.
(87) Kahn, O. *Molecular Magnetism*; VCH: New York, 1993.
(88) Sage, J. T.; Xia, Y.-M.; Debrunner, P. G.; Keough, D. T.; de Jersey, J.; Zerner, B. *J. Am. Chem. Soc.* **1989**, *111*, 7239.
(89) Guigliarelli, B.; Bertrand, P.; Gayda, J. P. *J. Chem. Phys.* **1986**, *85*, 1699.

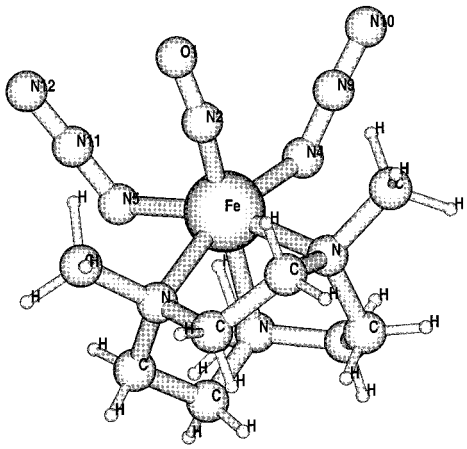

Figure 7. The $FeLNO(N_3)_2$ complex. The positional parameters correspond to the crystallographic structure of Pohl and Wieghardt.[44]

5. Density Functional Theory of a $\{FeNO\}^7(S = {}^3/_2)$ Complex

To interpret some Mössbauer results we have performed electronic structure calculations on a monomeric iron complex containing the $\{FeNO\}^7$ motif. Pohl and Wieghardt[44] have reported $FeL(NO)(N_3)_2$ ($L = C_9H_{21}N_3$) as the first crystallographically characterized octahedral $\{FeNO\}^7$ complex with a quartet ground state (Figure 7). The tridentate macrocycle $(CH_3)_3TACN$ is facially coordinated. The complex is paramagnetic and displays a room temperature magnetic moment of 4.06 μ_B. The temperature dependence of its magnetic susceptibility, in the 100 to 298 K range, obeys the Curie−Weiss law. The complex has been classified as a $\{FeNO\}^7(S = {}^3/_2)$ type that does not display spin-crossover.[44] Debrunner et al.[90] performed 4.2 K Mössbauer measurements on $FeL(NO)(N_3)_2$ and determined parameters characteristic of $\{FeNO\}^7(S = {}^3/_2)$ complexes (i.e., $\delta_{Fe} = 0.62$, $\Delta E_Q = 1.31$ mm/s).

We have applied Kohn−Sham density functional theory to study $FeL(NO)(N_3)_2$. Although we have performed an extensive computational study of the complex, in this work we limit ourselves to present results that are more relevant to the interpretation of Mössbauer parameters. Both, pure (i.e., U-BLYP, U-BPW91) and hybrid (i.e., U-B3LYP, U-B3PW91) density functional methods were used. The trends reported here are, in general, common to all methods, and we mainly limit our discussion to results obtained from a U-BPW91/6-311G* model.

In general, the unrestricted Kohn−Sham wavefunctions are eigenfunctions of $\mathbf{S}_z$ but are not eigenfunctions of the total spin operator $\mathbf{S}^2$. As a consequence, the quartet-state single-determinant wavefunction can include admixtures from other spin states. Such an admixture implies that the quartet wavefunction is spin-contaminated, mostly from the higher sextet. In the present case the spin contamination is not large since the calculated (U-BPW91/6-311G*) values of the total spin operator are $\langle S^2\rangle_B \approx 4.01$ and $\langle S^2\rangle_A \approx 3.77$. The subscripts B and A stand for before and after annihilation of the first spin contaminant, respectively.[91,92] These values can be compared, for example, to results we obtained for the corresponding U-HF/6-311G* wavefunction which yielded $\langle S^2\rangle_B \approx 4.81$ and $\langle S^2\rangle_A \approx 4.43$.

Energies and Composition of Molecular Orbitals. Figure 9 shows the energies and main composition of some frontier molecular orbitals. Convergence to a quartet state imposed the occupation of 91α and 88β molecular orbitals. The unrestricted calculations allowed α and β electrons to have different spatial localization and exchange interactions between majority spin (α) electrons lowered their energy with respect to the corresponding minority (β) electrons. These trends are only altered for the unoccupied orbitals of L ($C_9H_{21}N_3$) character which being substantially higher in energy have α and β labels of similar composition and energy. Orbitals 86β and 87β are fairly close in energy, appearing almost degenerate in the scale of the figure.

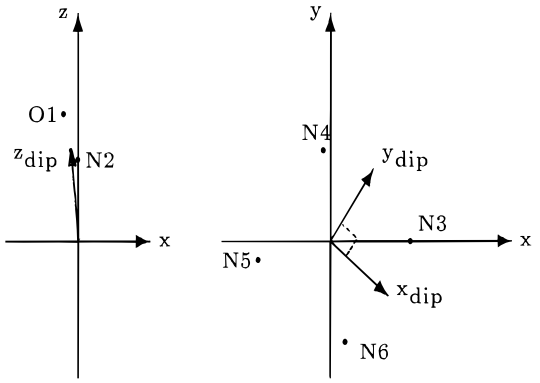

Figure 8. Coordinate system $\hat{o}(x, y, z)$ with origin at the iron site of $FeLNO(N_3)_2$. The Fe−N2(O) bond defines the z axis and the x coordinate of N3 defines the x axis. $\hat{o}(x, y, z)$ is the reference for describing molecular orbitals and natural atomic orbitals obtained from DFT calculations. The calculated orientations of $\tilde{a}_{dip}$ are also shown. z_{dip} and x_{dip} are rotated 4.1−7.3° with respect to z and 38° with respect to x.

The composition of the frontier molecular orbitals (MOs) provides significant insight about the nature of the Fe−NO bond. In what follows, we briefly discuss the composition of some frontier orbitals corresponding to the $S = {}^3/_2$ U-BPW91/6-311G* wavefunction with respect to a coordinate system where iron is at the origin and the z axis is defined by the Fe−N_2 bond (Figures 7 and 8). The azido ligands are referred as $(N_3)_A$ (i.e., N_5, N_{11}, N_{12}) and $(N_3)_B$ (i.e., N_4, N_9, N_{10}).

The molecular orbital description of diatomics such as the free NO radical has been discussed extensively in the literature. For the interpretation of our results we simply note that the frontier orbitals of the free ligand include two π-antibonding interactions between nitrogen and oxygen, only one of which is occupied. Upon complexation, with respect to our coordinate system, these two orbitals are composed of atomic orbitals of p_x or p_y symmetry and are referred in this work as NO $\pi^*(p_x)$ and NO $\pi^*(p_y)$, respectively. MOs 86α, 87α, 88α, 88β, and 89α of $FeL(NO)(N_3)_2$ are mainly localized on the two azido ligands with main composition given in Table 5 and Figure 9. MO 89β is the LUMO, essentially a metal orbital of d_{xy} symmetry.

Occupied MO 86β is delocalized throughout three fragments of the molecule. It has main contributions from the NO ligand (24.9%), $(N_3)_B$ (23.8%), and the iron ion (19.8%). There is also a smaller contribution from the other azido ligand. As shown in Figure 10, there is a strong π-bonding interaction between Fe(d_{yz}) and NO $\pi^*(p_y)$. The contribution from the azido nitrogen bound to iron, which has a hybridized sp character, lies on the yz plane and displays some bonding character with respect to the metal. The two-dimensional contour is a slice in the yz plane and shows the overlap between metal and ligand orbitals.

Occupied MO 87β is delocalized throughout three fragments of the molecule. It has main contributions from the NO ligand (24.9%), $(N_3)_A$ (24.3%) and the iron ion (22.3%). There is a

(90) See footnote 4 of ref 21 et al.
(91) Schlegel, H. B. *J. Chem. Phys.* **1986**, *84*, 4530.
(92) Schlegel, H. B. *J. Phys. Chem.* **1988**, *92*, 3075.

Table 5. Energies (ϵ) and Percent Composition of Frontier Molecular Orbitals Obtained from $S = {}^3/_2$ U-BPW91/6-311G* Wavefunction of $FeL(NO)(N_3)_2$ ($L = C_9H_{21}N_3$)[a]

		MO									
ligand	atom	86α O	87α O	88α O	89α O	90α O	91α O	92α V	93α V	94α V	95α V[b]
	Fe1	18.3	12.1	1.9	12.8	30.6	28.3	9.6	16.9	3.3	1.9
NO	N2	0.0	0.3	0.1	0.6	13.9	1.0	41.1	34.7	0.3	0.4
	O1	0.2	0.3	0.1	0.3	9.5	0.9	30.5	23.6	0.1	0.1
$(N_3)_A$	N5	13.6	12.7	12.0	20.1	3.8	7.9	1.5	2.4	0.1	0.0
	N11	1.3	0.8	0.2	0.3	0.4	0.6	0.5	0.8	0.3	0.0
	N12	6.5	8.2	9.7	18.2	3.6	7.3	0.5	2.4	0.3	0.0
$(N_3)_B$	N4	12.3	16.0	23.9	8.1	2.9	9.2	2.2	1.4	0.1	0.2
	N9	1.0	1.0	0.3	0.1	0.8	0.6	1.3	0.6	0.2	0.1
	N10	5.5	9.5	20.0	7.2	2.4	8.1	0.6	1.5	0.3	0.1
		ϵ (eV)									
		−5.503	−5.287	−4.676	−4.577	−4.117	−3.824	−2.427	−2.174	+0.264	+0.676
		MO									
ligand	atom	86β O	87β O	88β O	89β V	90β V	91β V	92β V	93β V	94β V	95β V
	Fe1	19.8	22.3	0.7	48.8	39.1	30.7	44.6	40.5	2.9	1.7
NO	N2	11.7	11.2	0.5	0.2	19.9	25.0	1.8	14.6	0.3	0.4
	O1	13.2	13.7	0.5	0.1	13.2	15.7	1.0	7.1	0.1	0.1
$(N_3)_A$	N5	2.3	15.4	20.7	2.0	3.3	1.4	3.8	1.7	0.1	0.0
	N11	0.1	2.0	0.3	0.9	3.1	0.8	2.4	2.4	0.2	0.0
	N12	1.4	6.9	16.9	4.2	0.4	0.1	5.0	3.6	0.2	0.0
$(N_3)_B$	N4	15.0	0.6	16.3	2.4	3.6	2.9	4.2	1.7	0.1	0.2
	N9	2.2	0.2	0.2	1.4	3.5	2.3	2.4	2.6	0.2	0.1
	N10	6.6	0.3	13.2	4.9	1.0	0.3	4.6	3.5	0.2	0.1
		ϵ (eV)									
		−4.683	−4.666	−4.476	−2.860	−2.426	−2.205	−1.762	−1.238	+0.272	+0.684

[a] The total percent contributions of L to any MO can be determined by subtracting from 100% the sum of the contributions listed in this table. [b] O and V represent occupied and virtual (unoccupied) MOs, respectively.

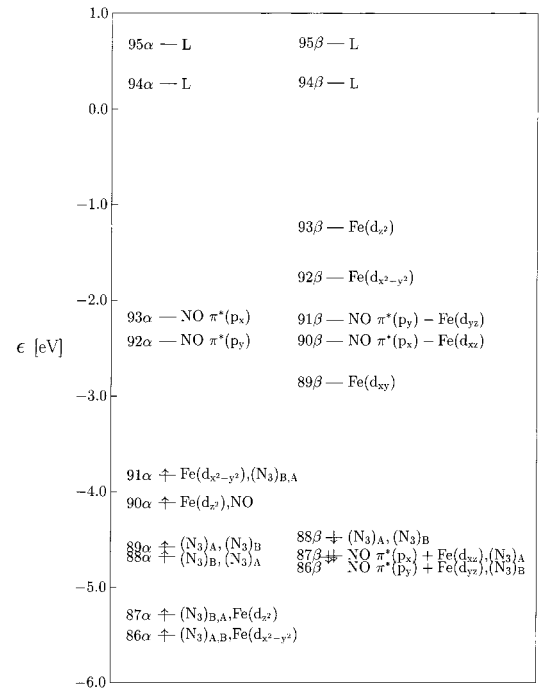

Figure 9. Energies and main composition of frontier molecular orbitals obtained from a U-BPW91/6-311G* calculation on $FeLNO(N_3)_2$. Orbital energies are given in Table 5. The + and − signs indicate symmetric and antisymmetric combinations of metal and NO orbitals, respectively.

strong π-bonding interaction between Fe(d_{xz}) and NO $\pi^*(p_x)$. The contribution from the azido nitrogen bound to iron, which has some hybridized sp character, lies in, the *xz* plane and has some bonding character with respect to the metal (Figure 11). The two-dimensional contour is a slice in the *xz* plane and shows the overlap between metal and ligand orbitals.

Occupied MO 90α is mainly centered on the iron ion (30.6%) with dominant d_{z^2} symmetry and a lesser contribution from s orbitals. The NO ligand also contributes significantly to this orbital (23.4%), and its nitrogen has a mixture of s and p electron densities. The terminal oxygen has p-type density which acquires an incipient bonding character with respect to the metal via the hybridized orbital of nitrogen. This combination of orbitals allows some delocalization within the $\{FeNO\}^7$ unit (Figure 12). There is also a σ-antibonding interaction between the metal orbital and the p_z orbital from the axial L nitrogen. The σ-type interactions between the metal and the axial ligands raise the energy of this MO with respect to the metal-centered π-type α orbitals.

Virtual MO 90β is almost equally distributed between the iron ion (39.1%) and the NO ligand (33.1%). This orbital corresponds to the strong π-antibonding interaction between Fe-(d_{xz}) and NO $\pi^*(p_x)$. There are also minor contributions from the azido and L ligands. This antibonding MO is destabilized with respect to its bonding counterpart (MO 87β) by 2.24 eV (Figure 13).

Occupied MO 91α is the HOMO. Its main contribution comes from a metal orbital of $d_{x^2-y^2}$ symmetry (28.3%). The iron orbital is σ-antibonding with all four equatorial nitrogens. Such combined antibonding interaction in the *xy* plane destabilizes MO 91α which is highest in energy among the α-occupied metal centered orbitals (Figure 14).

Virtual MO 91α has main contributions from the NO ligand (40.7%) and the iron ion (30.7%). This orbital corresponds to the strong π-antibonding interaction between Fe(d_{yz}) and NO $\pi^*(p_y)$. MO 91β is destabilized with respect to its corresponding π-bonding orbital (MO 86β) by ∼2.48 eV (Figure 15).

We finally mention that the main occupied molecular orbitals involved in σ ligand (NO) to metal donation are considerably lower in energy than those listed in Table 5. In particular, MOs

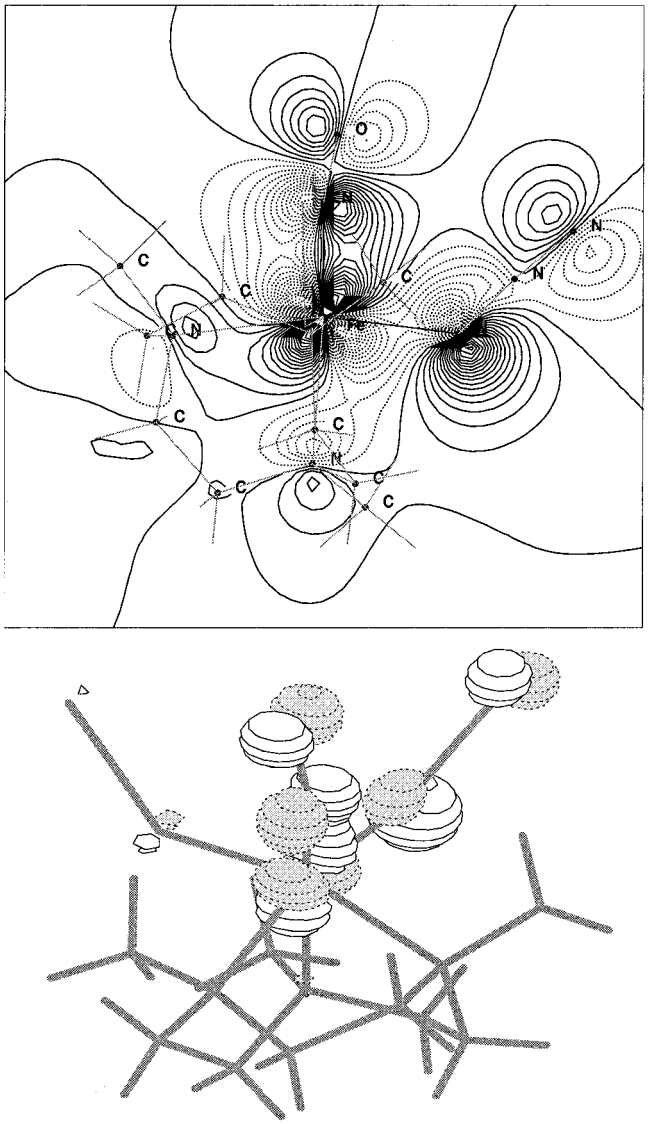

Figure 10. MO 86β of FeLNO$(N_3)_2$. (Top) Isovalue contour plot obtained at the U-BPW91/6-311G* level. The plot is in the *yz* plane and shows the π-bonding interaction between Fe(d_{yz}) and NO π^*(p_y). (Bottom) Three-dimensional representation.

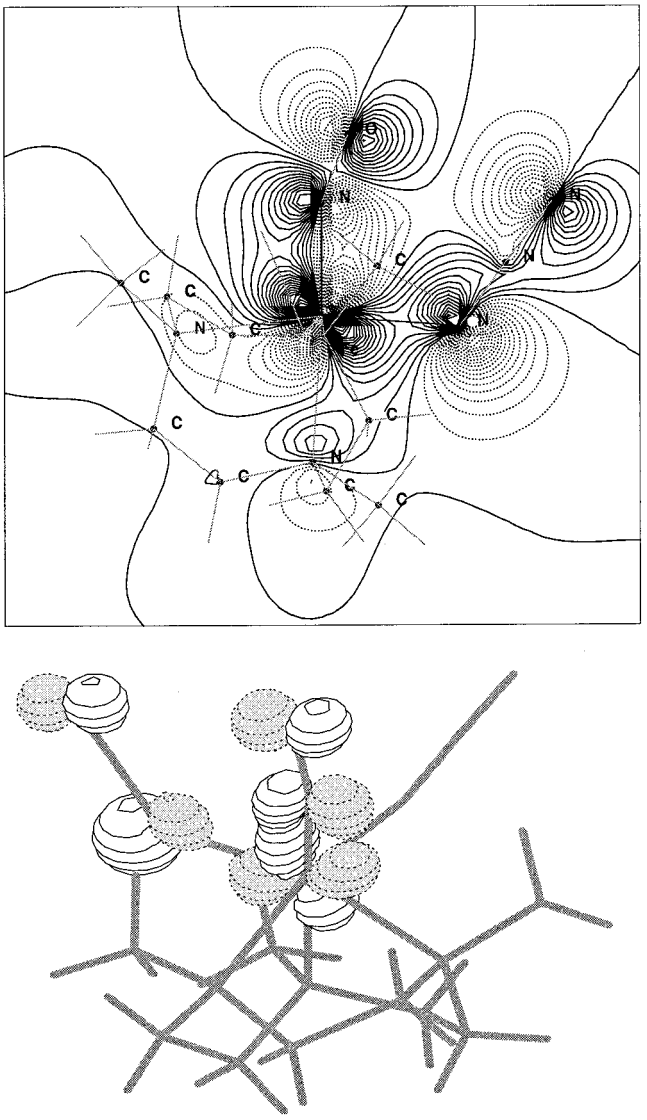

Figure 11. MO 87β of FeLNO$(N_3)_2$. (Top) Isovalue contour plot obtained at the U-BPW91/6-311G* level. The plot is in the *xz* plane and shows the π-bonding interaction between Fe(d_{xz}) and NO π^*(p_x). (Bottom) Three-dimensional representation.

45α, β (not shown) and 54α, β (Figure 16) are mainly localized on the ligand and form σ-bonding combinations with Fe(d_{z^2}). These MOs also have some contribution from iron 4s orbitals. In regards to the magnetic properties of the complex, one important result is that the spatial localizations of MOs 45α and 45β are virtually identical. This is also true for MOs 54α and 54β. Therefore, the σ ligand to metal donation that occurs via these MOs does not carry any significant transfer of spin density.

Atomic Charge and Spin Densities. The atomic charges corresponding to the quartet U-BPW91 wavefunction are listed in Table 6. The main trends in charge distribution were common to the four combinations of exchange-correlation functionals. Pure density functional methods (i.e., U-BLYP, U-BPW91) produced, in general, slightly less charge polarization than hybrid methods (i.e., U-B3LYP, U-B3PW91). This trend was only altered for the atomic charges of NO which are slightly more negative for U-BPW91 than U-B3PW91. The NPA analysis assigned most of the positive charge to the iron ion (+1.358) and lesser positive charges to the central azido nitrogens (N9: +0.172, N11: +0.166). By contrast, the azido nitrogens bound to the metal have substantial negative charge (i.e., N4: −0.616, N5: −0.602). The negative charges of the L nitrogens are of nearly equal magnitude with an average value of −0.561 units. The negative charge of the NO ligand is small with oxygen (−0.158) being more negatively charged than nitrogen (−0.095), consistent with their different electronegativities. The nearly neutral character of the nitrogen belonging to NO contrasts greatly with the negative charge of the other five nitrogens bound to the metal. These observations reflect the strong delocalization of charge within the $\{FeNO\}^7$ unit in comparison to the more localized charge of the N_3 and L ligands.

In order to characterize the spin structure of the complex, it is important to consider the spatial distribution of its spin density (Table 6). The total calculated molecular spin is +3 units. This is a necessary result from the self-consistent field calculations that imposed convergence to a quartet state. The relative spin densities, however, reflect the highly covalent nature of the $\{FeNO\}^7$ unit that allows for some, but not full, spin polarization. The net α spin at the iron ion (+2.909) approaches the +3 units of spin that correspond to an idealized Fe($S = {}^3/_2$) configuration. There is also some net α spin associated with

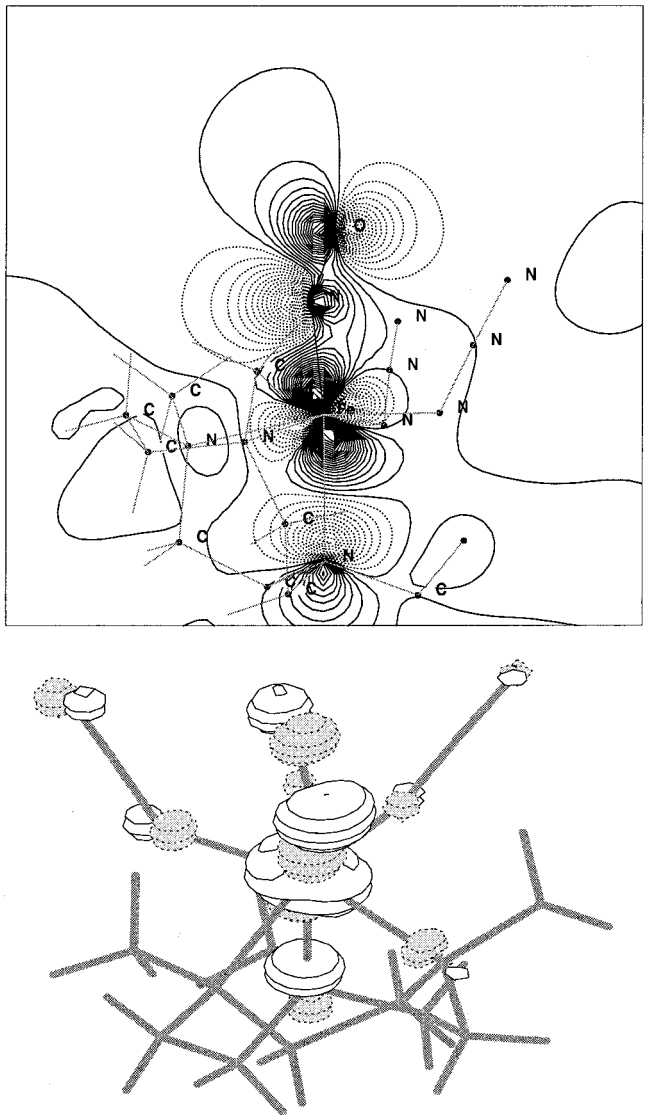

Figure 12. MO 90α of FeLNO$(N_3)_2$. (Top) Isovalue contour plot obtained at the U-BPW91/6-311G* level. The plot is in the Fe−N−O plane and shows the σ interactions between Fe(d_{z^2}) and the axial ligands. (Bottom) Three-dimensional representation.

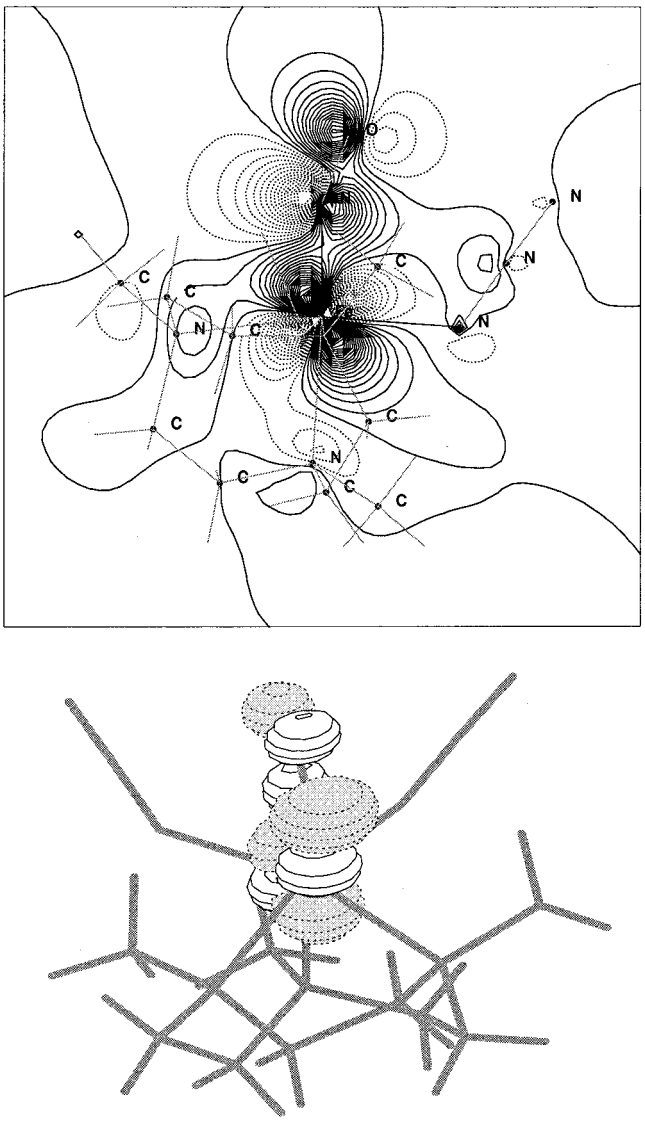

Figure 13. MO 90β of FeLNO$(N_3)_2$. (Top) Isovalue contour plot obtained at the U-BPW91/6-311G* level. The plot is in the *xz* plane and shows the π-antibonding interaction between Fe(d_{xz}) and NO π*-(p_x). (Bottom) Three-dimensional representation.

the azido ligands (i.e., $(N_3)_A$: +0.160, $(N_3)_B$: +0.192). The L ligand does not exhibit significant spin density and is essentially diamagnetic. Most of the β spin is localized on NO. However, the net spin of this ligand (−0.424) is between the 0 and −1 units corresponding to idealized singlet ($S = 0$) and doublet ($S = {}^1/_2$) states, respectively. Thus, the NO ligand can not be adequately classified according to either of these spin configurations since it does not host (nearly) whole units of β spin. The unusual spin densities, assigned to iron and NO are, to a large extent, a consequence of the delocalized character of MOs 86β and 87β. This is in contrast to open-shell complexes with valence molecular orbitals which are mainly centered on the metal or the radical ligand and, therefore, can attain nearly full spin polarization.[93] We notice that the hybrid methods (e.g., U-B3PW91) allowed for somewhat greater spin polarization; however, these methods also showed the delocalized character of some MOs as has been described for U-BPW91.

Table 6 shows that the net spin densities of iron and NO have opposite signs. This is a consequence of the significant overlap between Fe(d_{xz}, d_{yz}) and NO π*(p_x, p_y) orbitals which gives rise to spin pairing. Nevertheless, one should distinguish between two situations: (i) The present case where due to the highly delocalized nature of some MOs the complex can not attain full spin polarization and, therefore, can not be adequately classified as either Fe($S = {}^5/_2$) antiferromagnetically coupled to NO($S = 1$) or Fe($S = 2$) antiferromagnetically coupled to NO($S = {}^1/_2$). (ii) Cases where the overlap between metallic and organic paramagnetic centers is relatively minor, allowing for spin coupling but at the same time for nearly full spin polarization. In these situations the two paramagnetic centers have spin densities with distinctly different spatial localization and can be classified according to idealized configurations which are very nearly represented by calculated spin densities.

Natural Atomic Orbitals. A population analysis in terms of natural atomic orbitals[70,71,73] (NAO) provides additional insight about the origin of the spin distributions within the {FeNO}^{7} unit. Table 7 shows the corresponding occupancies and net spin.

All valence NAOs of iron have net α spin. NAOs $3d_{xy}$, $3d_{x^2-y^2}$ and $3d_{z^2}$, in that order, have the greatest α character. This

(93) Adams, D. M.; Noodleman, L.; Hendrickson, D. N. *Inorg. Chem.* **1997**, *36*, 3966.

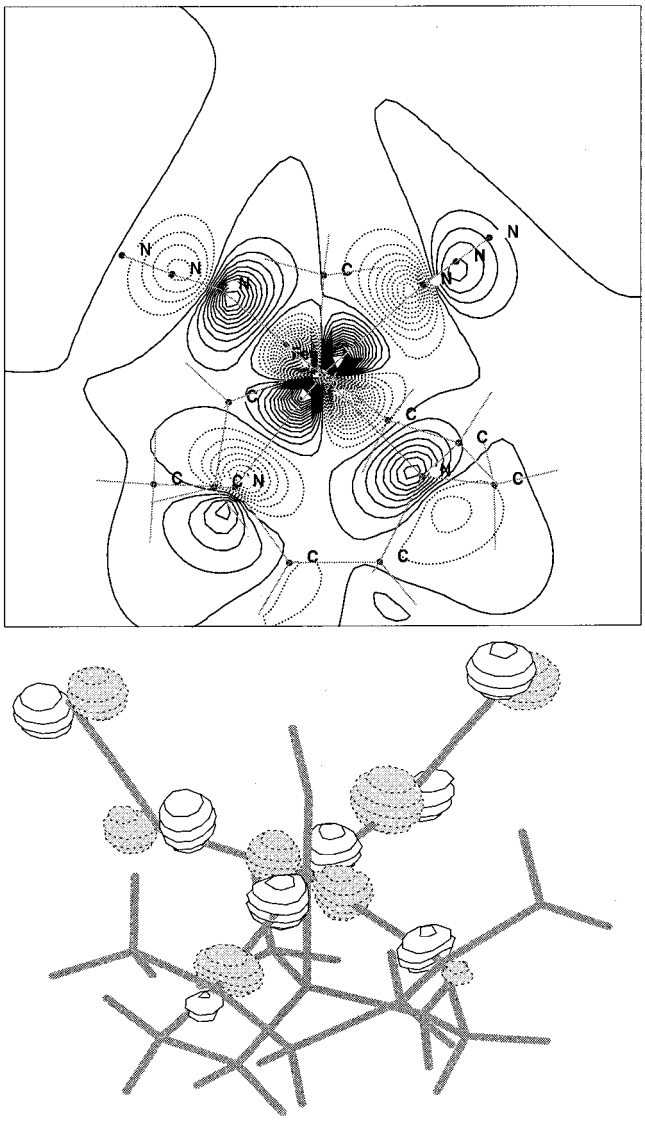

Figure 14. MO 91α of $FeLNO(N_3)_2$. (Top) Isovalue contour plot obtained at the U-BPW91/6-311G* level. The plot is slightly above the *xy* plane and shows the σ-antibonding interaction between $Fe(d_{x^2-y^2})$ and the four equatorial nitrogens. (Bottom) Three-dimensional representation.

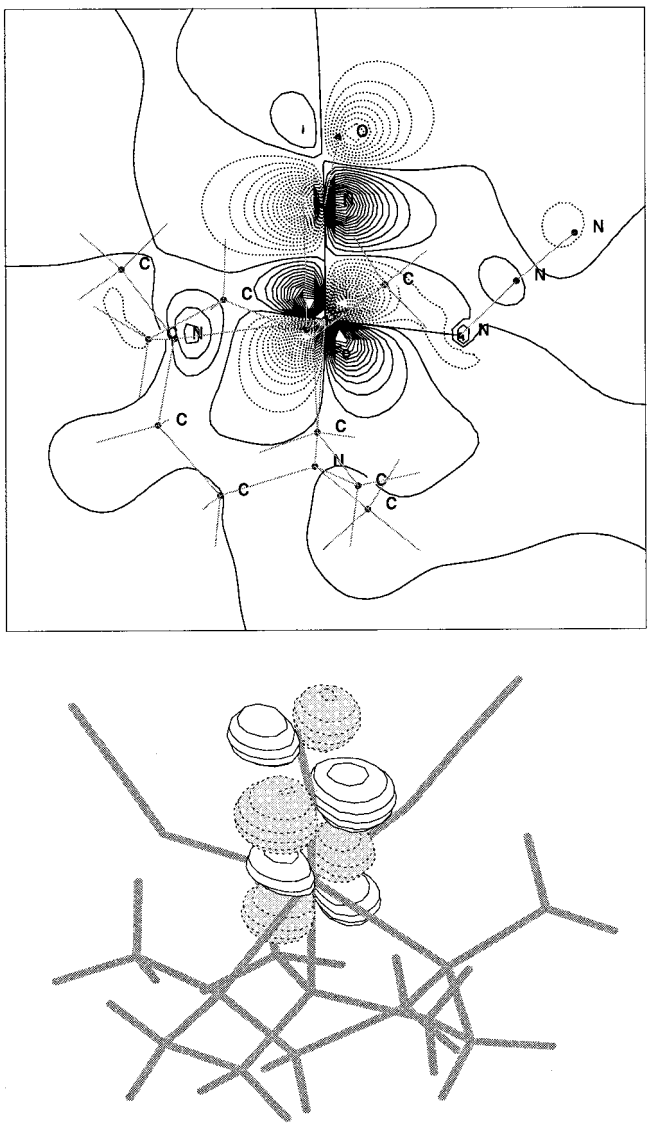

Figure 15. MO 91β of $FeLNO(N_3)_2$. (Top) Isovalue contour plot obtained at the U-BPW91/6-311G* level. The plot is in the *yz* plane and shows the π-antibonding interaction between $Fe(d_{yz})$ and NO π^*-(p_y). Bottom: Three-dimensional representation.

provides insight about the spatial localization of most of the metallic spin. From these three NAOs, $3d_{z^2}$ has the largest β occupancy (0.278) as reflected by its relatively low net spin. NAOs $3d_{xz}$, and $3d_{yz}$ have the greatest occupancy but the lowest net spin indicating that these orbitals have significant β occupancy.

The idealized configurations for high-spin ferric and high-spin ferrous ions in octahedral environments are $t_{2g}^3\, e_g^2 (S = {}^5/_2)$ and $t_{2g}^4\, e_g^2 (S = 2)$, respectively. While the former oxidation state is expected to have five half-occupied ligand field (d) orbitals, the latter is expected to have one doubly occupied and four half-occupied ligand field (d) orbitals. The occupancies and net spin of the metallic NAOs indicate that the electronic configuration of iron in $FeL(NO)(N_3)_2$ is different from either of these idealized ligand field configurations. One main difference arises from the nearly equal occupancy (∼1.4) of NAOs $3d_{xz}$ and $3d_{yz}$ which can not be readily classified as either singly or doubly occupied. The combined α and β occupancy of NAOs $3d_{xz}$ and $3d_{yz}$ also lowers substantially the total metallic spin density (+2.909 units) relative to idealized high-spin ferric (+5 units) or high-spin ferrous (+4 units) configurations. Within the molecular orbital framework used in this work, the previous observations also follow from the combined metal and ligand character of occupied MOs 86β and 87β. The delocalization of these orbitals appears to preclude the assignment of formal oxidation states which are appropriate for more ionic environments.

The p NAOs of NO have small net β spin since their β occupancies are only slightly larger than their α occupancies. We notice, however, that NAOs $N2(p_y)$ and $O1(p_y)$ have a somewhat larger β occupation. NAO 2s has a slight α character suggesting delocalization from the metal, perhaps from NAO $3d_{z^2}$ as follows from the description given for MO 90α.

6. Discussion

Magnitude of δ_{Fe} in $\{FeNO\}^7 (S = {}^3/_2)$ Sites. Mössbauer isomer shifts are very sensitive to the electronic environment of high-spin ferric, high-spin ferrous, and quartet-state iron nitrosyl sites. The marked effects of NO binding on ^{57}Fe isomer

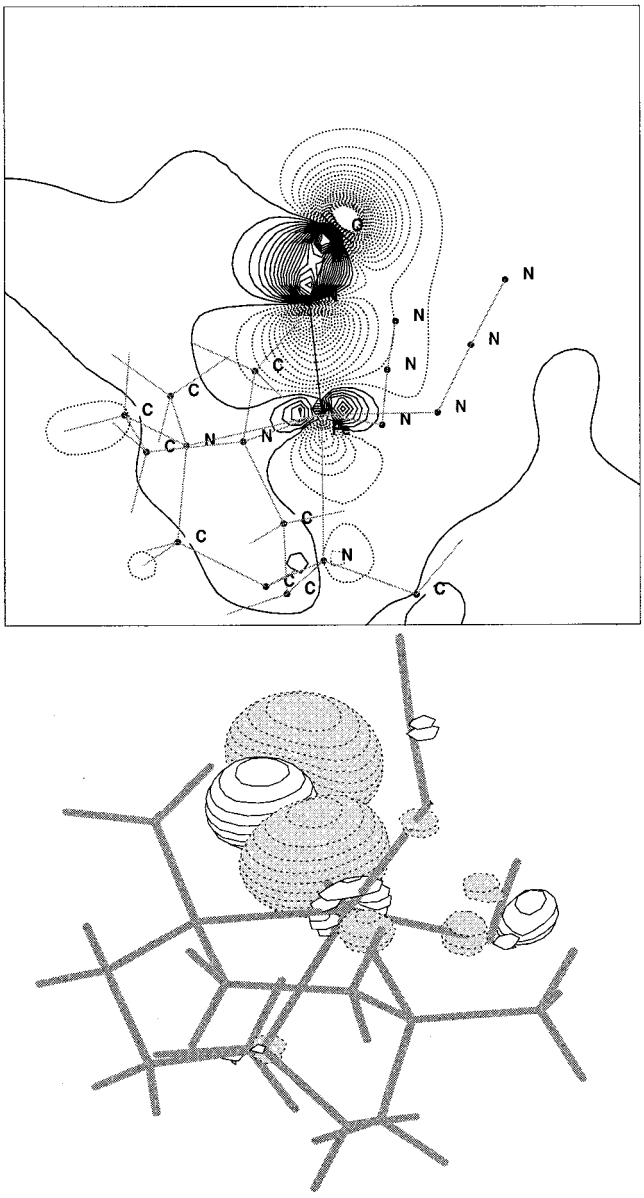

Figure 16. MO 54α of $FeLNO(N_3)_2$. (Top) Isovalue contour plot obtained at the U-BPW91/6-311G* level. The plot is in the Fe−N−O plane and shows the ∇-bonding interaction between NO(p_z) and Fe-(d_{z^2}, 4s). (Bottom) Three-dimensional representation.

Table 6. Atomic Charge and Spin Densities of $FeL(NO)(N_3)_2$ (L = $C_9H_{21}N_3$) Obtained from NPA[73] Analysis of $S = {}^3/_2$ U-BPW91/6-311G* Wavefunction

ligand	atom	charge	spin
	Fe	+1.358	+2.909
NO	N2	−0.095	−0.205
	O1	−0.158	−0.219
$(N_3)_A$	N5	−0.602	+0.044
	N11	+0.166	−0.005
	N12	−0.233	+0.121
$(N_3)_B$	N4	−0.616	+0.064
	N9	+0.172	−0.009
	N10	−0.231	+0.137
$C_9H_{21}N_3$	N3	−0.562	+0.064
	N6	−0.560	+0.057
	N7	−0.561	+0.025

shifts have long been recognized.[94] To interpret differences between isomer shifts from various electronic environments it is helpful to consider that these are, to within a constant, the product of nuclear ($\langle R^2\rangle_e - \langle R^2\rangle_g$) and electronic ($|\psi_s(O)|^2_{Absor} - |\psi_s(O)|^2_{Sour}$) terms.[74,95,96] In Mössbauer experiments the s electron density at the source nucleus ($|\psi_s(O)|^2_{Sour}$) remains constant, whereas the s electron density at a particular absorber ($|\psi_s(O)|^2_{Absor}$) can change with electronic environment. The shielding produced by 3d electrons on s electrons, in particular on the 3s shell, diminishes the electronic charge at the iron nucleus and, consequently, increases the isomer shifts. Conversely, an increment in 3s electron density due to a reduction of d electron shielding has been reported for some iron−nitrosyl complexes.[94] Therefore, we can correlate greater 3d electron populations with larger isomer shifts and lesser 3d populations with smaller isomer shifts.

Table 7. NAO Occupancies and Net Spin for $\{FeNO\}^7$ Unit of $FeL(NO)(N_3)_2$[a]

atom	NAO	occupancy	spin
Fe	4s	0.302	+0.011
	$3d_{xy}$	1.170	+0.804
	$3d_{xz}$	1.415	+0.426
	$3d_{yz}$	1.401	+0.376
	$3d_{x^2-y^2}$	1.225	+0.720
	$3d_{z^2}$	1.124	+0.569
N2	2s	1.548	+0.035
	$2p_x$	1.224	−0.063
	$2p_y$	1.167	−0.154
	$2p_z$	1.089	−0.022
O1	2s	1.702	−0.003
	$2p_x$	1.512	−0.056
	$2p_y$	1.481	−0.136
	$2p_z$	1.436	−0.023

[a] Obtained from NPA analysis of $S = {}^3/_2$ U-BPW91/6-311G* wavefunction.

The results from density functional theory presented in section 5 provide insight about the origin of the unusual isomer shifts measured for $\{FeNO\}^7(S = {}^3/_2)$ sites. We found that some molecular orbitals allow strong valence delocalization between metal and nitrosyl orbitals. This is particularly true for some MOs with substantial atomic orbital composition of d_{xz} and d_{yz} symmetry, and as a result, the corresponding NAOs have fairly large occupancies (Table 7). Since the individual occupancies of $\{FeNO\}^7(d_{xz}, d_{yz})$ orbitals are higher than what is expected for high spin ferric ions, the associated shielding effect explains, to a large extent, the larger isomer shifts of the former relative to those of the latter.

An analogous argument can explain the somewhat smaller isomer shifts of $\{FeNO\}^7$ sites relative to Fe^{2+} ions. The combined effects of Fe−NO π-delocalization and σ-donation apparently yield an s electron charge at the iron nucleus that is greater than the corresponding electronic charge of ferrous ions. The total d occupancy shown in Table 7, which reflects the effects of π-delocalization, initially suggests that significant shielding on 3s electrons would produce isomer shifts almost comparable to those of ferrous ions. However, one should also consider direct ligand delocalization towards the metallic 4s shell, in particular the effects of σ-donation from the NO ligand. In section 5 we found that the molecular orbitals involved in σ-donation, although of dominant NO character, also have some metallic composition of d_{z^2} and s symmetry. The corresponding delocalization should increase the 4s charge density and lower

(94) Danon, J. *J. Chem. Phys.* **1963**, *39*, 236.

(95) Srivastava, J.; Bhargara, S.; Iyengar, P.; Thosar, B. In *Advances in Mössbauer Spectroscopy*; Thosar, B., Iyengar, P., Eds.; Elsevier; New York, 1983.

(96) Cohen, R. L. In *Applications of Mössbauer Spectroscopy*; Cohen, R. L., Ed.; Academic Press: New York, 1976; Vol. 1.

the isomer shifts. This is reflected by the occupancy of about 0.3 units assigned to the 4s shell by the NAO analysis of FeL(NO)$(N_3)_2$. Therefore, the effects of shielding due to π-delocalization are to some extent moderated by σ-donation. We notice that a 0.3 occupancy for a 4s shell is not necessarily higher than that for other iron configurations. However, the reduction in isomer shifts due to a direct contribution of 4s electrons to $|\psi_s(0)|^2$ is greater than the opposing enhancing effect, which occurs via the indirect mechanism of shielding, of an equivalent occupancy of 3d electrons.[97−99]

The net effect of the various Fe−NO orbital interactions can be summarized with the following relation for the electronic charge at the iron nuclei:

$$|\psi_s(0)|^2_{Fe^{3+}(S=5/2)} > |\psi_s(0)|^2_{\{FeNO\}^7(S=3/2)} > |\psi_s(0)|^2_{Fe^{2+}(S=2)}$$

Magnitude of ΔE_Q in $\{FeNO\}^7$($S = 3/2$) Sites. Considering the strong valence electron delocalization within the iron nitrosyl units it is surprising that their quadrupole splittings are not particularly large. One would initially expect a substantial valence contribution to the EFG giving rise to fairly large values of ΔE_Q. However, the representative values shown in Table 2 reveal that this parameter can take relatively low values (e.g., $0.58 \lesssim |\Delta_{E_Q}| \lesssim 1.67$) in comparison to, for example, high-spin ferrous ions. To interpret these results we recall that ΔE_Q is proportional to the expectation value of the principal axis component $\langle V_{zz}\rangle$ of the EFG tensor. The valence contribution to the EFG differs according to the symmetry of each d orbital. An approximate knowledge of the orbital occupancies (n_i) allows us to estimate the expectation value

$$\langle V_{zz}\rangle^{Val} \approx \sum_i^5 n_i \langle V_{zz}\rangle_i \qquad (16)$$

where $\langle V_{zz}\rangle_i$ correspond to each d orbital. Equation 10 shows that $\langle V_{ii}\rangle$ are proportional to the expectation values of $\langle L_i^2 - 2\rangle$ given in Table S1. Since we obtained the NAO occupancies for FeL(NO)$(N_3)_2$ we can estimate $\langle V_{zz}\rangle^{Val}$ for this complex. From Table 7 and eq 16 it follows that $\langle V_{zz}\rangle^{Val}/4e(1 - R)\langle r^{-3}\rangle \approx 0.170(1/7) - 0.415(1/14) - 0.401(1/14) + 0.225(1/7) - 0.124(1/7) \approx -0.137(1/7)$, where we have approximated $\langle r^{-3}\rangle$ as being equal for all electrons. The negative sign of $\langle V_{zz}\rangle^{Val}$ matches the negative values measured for other monomeric $\{FeNO\}^7$ complexes (Table 2) in contrast to the positive value determined for deoxyHrNO.

The previous analysis provides insight about the physical origin of the quadrupole splittings of $\{FeNO\}^7$ sites and can be extended to other iron configurations to gain insight about their own characteristic values. The nominal value of $\langle V_{zz}\rangle^{Val}/4e(1 - R)\langle r^{-3}\rangle$ corresponding to $Fe^{3+}(S = 5/2)$ is 0, whereas for $Fe^{2+}(S = 2)$, assuming a d_{xy} ground state, this value is $+1/7$. This can be seen from Table S1 which shows that the combined expectation value of $\langle L_z^2 - 2\rangle$ for the $d^{\uparrow}_{xy}\, d^{\uparrow}_{xz}\, d^{\uparrow}_{yz}\, d^{\uparrow}_{z^2}\, d^{\uparrow}_{x^2-y^2}$ configuration vanishes, whereas for $d^{\uparrow\downarrow}_{xy}\, d^{\uparrow}_{xz}\, d^{\uparrow}_{yz}\, d^{\uparrow}_{z^2}\, d^{\uparrow}_{x^2-y^2}$ it has a finite value corresponding to the extra d electron. Therefore, we can establish the following inequality for the expectation values of the valence EFG of the various electronic configurations:

$$0 \approx |\langle V_{zz}\rangle^{Val}_{Fe^{3+}(S=5/2)}| \lesssim |\langle V_{zz}\rangle^{Val}_{\{FeNO\}^7(S=3/2)}| < |\langle V_{zz}\rangle^{Val}_{Fe^{2+}(S=5/2)}|$$

Table S1 helps to illustrate that even though quadrupole splittings of $Fe^{3+}(S = 5/2)$ and $\{FeNO\}^7(S = 3/2)$ sites can take similar values, these arise from different electronic configurations. In both cases, the relatively low quadrupole splittings are related to the mutual cancellation of the valence orbital contributions to the EFG even though their d orbital occupancies have important differences as pointed out in section 5. When valence contributions to the EFG are small the relative importance of lattice contributions is greater. To some extent the spread in quadrupole splittings illustrated by Table 2 should arise from somewhat different ligand environments that produce distinct lattice EFGs.

Table 1 reveals that the quadrupole splitting of $\{FeNO\}^7$ in deoxyHrFNO remains constant in a 50 to 250 K range. Such temperature independence has also been observed in other iron nitrosyl complexes with quartet ground state. For example, Wells et al.[29] reported Mössbauer parameters for [Fe(5-Cl-salen)NO] (Table 2) which are close to those of deoxyHrNO and an electric field gradient that exhibits no temperature dependence. These observations indicate that the EFG at these iron sites originates mainly from temperature independent lattice contributions with little contribution from the valence.

Magnetic Hyperfine Tensors of $\{FeNO\}^7$ Sites. The origin of the intrinsic hyperfine anisotropy for the $S = 3/2$ site of deoxyHrNO is not immediately obvious since the iron within its $\{FeNO\}^7$ group does not have the configuration of a pure ion. Furthermore, in deoxyHrNO the intrinsic complexity in understanding the origin of the hyperfine interaction of an isolated $\{FeNO\}^7$ unit is further complicated by its coupling to the Fe^{2+} site which can introduce additional sources of anisotropy from intramolecular electron delocalization.[25] As a first step in understanding the hyperfine structure within a spin-coupled system, we now discuss the origin of the hyperfine tensor of an isolated $\{FeNO\}^7$ site such as found in the FeL(NO)$(N_3)_2$ complex.

The main contributions to the hyperfine tensor can be represented by the following second-order expression [25,100,101]

$$a_{ii} = P[-\kappa + (g_{ii} - 2) + 1/14\,\langle L_i^2 - 2\rangle] \qquad (17)$$

where a_{ii} are the three components in the principal axes. In eq 17, $-\kappa$, $(g_{ii} - 2)$, and $1/14\langle L_i^2 - 2\rangle$ represent the dominant Fermi contact (core polarization), orbital, and dipolar contributions, respectively. While the first term is isotropic, the latter two are anisotropic. Furthermore, the orbital term can effectively reduce the absolute values of a_{ii} if $g_{ii} - 2 > 0$, but the dipolar term, being traceless, does not affect the value of $Tr\tilde{a}_i$.

The intrinsic parameters of Table 4 indicate that, within the sensibility of the method, $\tilde{g}^2$ is isotropic with an average equal to the spin-only value (i.e., $\sim$2). In this case the orbital contribution vanishes and $1/3 Tr\tilde{a}_2$ is equal to the Fermi contact contribution. This explains the high value of $1/3 Tr\tilde{a}$ determined for the $\{FeNO\}^7$ site in this work and also for some uncoupled sites.[35] The main source of anisotropy should arise from the dipolar term. The radial distributions of d electrons, as modified by anisotropic covalency, can introduce dipolar contributions.

The results from density functional theory (section 5) imply that strong electron delocalization via Fe(d_{xz})−NO*(p_x) and Fe(d_{yz})−NO*(p_y) bonding induce an anisotropic dipolar hyperfine

(97) Šimáneck, E.; Šroubek, Z. *Phys. Rev.* **1967**, *163*, 275.
(98) Watson, R. E.; Freeman, A. J. *Phys. Rev.* **1961**, *123*, 2027.
(99) Freeman, A. J.; Watson, R. E. In *Magnetism*; Rado, G. T., Suhl, H., Eds.; Academic Press: New York, 1965; Vol. 2A, Chapter 4, pp 167−305.
(100) Zimmermann, R. Ph.D. Thesis, Universität Erlangen-Nürnberg, Dresden, 1973.
(101) Abragam, A.; Price, M. H. L. *Proc. R. Soc. London* **1951**, *A205*, 135.

field. Table 7 shows that NAOs d_{xz} and d_{yz} have the greatest occupancy. From Table S1 it follows that these two NAOs will contribute the most to the componhents of the dipolar field which are proportional to $^1/_{14}\langle L_i^2 - 2\rangle$. In particular, $P^1/_{14}\langle L_x^2 - 2\rangle$ and $P^1/_{14}\langle L_y^2 - 2\rangle$ will acquire net positive values due to the large occupancies of d_{yz} and d_{xz}, respectively. By contrast, $P^1/_{14}\langle L_z^2 - 2\rangle$ will acquire a net negative value due to the combined occupancies of the same two NAOs (d_{xz} and d_{yz}). The contributions from NAOs d_{z^2} and $d_{x^2-y^2}$ tend to cancel each other since their occupancies are fairly close and their expectation values $\langle L_i^2 - 2\rangle$ have opposite signs. Therefore, the dipolar components in the *xy* plane oppose the Fermi contact term, whereas the axial component enhances it. This is in agreement with Mössbauer simulations for $S = {}^3/_2$ iron nitrosyl mononuclear complexes which are compatible with a larger a_{zz} relative to the other two components of the hyperfine tensor.[35]

To relate the orientation of the hyperfine tensor to the coordinate system used in DFT calculations (Figure 8) we followed the method implemented by Rega, Barone et al.[102−104] and used the molecular spin density $\rho^\alpha - \rho^\beta$ to determine the principal orientations of the dipolar hyperfine tensor ($\tilde{a}_{dip}$) for $FeL(NO)(N_3)_2$. The calculations show that a_{dip-zz} is nearly parallel to the $(-x,z)$ plane and rotated 4.1° (U-BPW91/6-311+G*) to 7.3° (U-B3PW91/6-311+G*) with respect to the *z* axis defined by the Fe−N2 bond.[105] At the same time, Mössbauer simulations for the mononuclear iron complexes IPNS−NO and EDTA−NO yielded a_{zz} components that are rotated by about 8 to 10° relative to the D_{zz} components.[35] These results suggest that the Fe−N2 (*z*) axis is fairly parallel to the D_{zz} axis.

Figure 6 shows that D_{2zz} and the largest hyperfine component a_{2xx}, have the same orientation (defined by z^2). Therefore, for the $\{FeNO\}^7$ site of deoxyHrNO the dipolar component also enhances the Fermi contact term in the axial direction. On the basis of the previous results for the mononuclear complexes, we have drawn an Fe−N(O) axis which is approximately parallel to the z_2 axis. The orientation of the ferrous tensor $\tilde{a}_1$ relative to the nuclear coordinates is less certain since its anisotropy arises from two contributions (orbital and dipolar) and the bridging OH^- is a relatively weak-field ligand.

Implications for the Electronic Structure of Non-Heme Iron Centers Involved in Dioxygen Activation. Some similarity between the electronic structures of nitric oxide and dioxygen give the first ligand an important role in studies that mimic the mechanism of activation of the second.[84,106] Several proteins have non-heme ferrous active sites which are known to react with nitric oxide and form stable complexes thiat include the $\{FeNO\}^7$ motif.[5,35] The results presented in this work are relevant for understanding the electronic structure of a variety of such complexes in mononuclear and binuclear enzymes. For example, much of our understanding of the electronic configuration of $\{FeNO\}^7$ sites should also apply to the mononuclear nitric oxide complexes of the enzymes putidamonooxin (PMO) and protocatechuate 4,5-dioxygenase (4,5-PCD) which also exhibit Mössbauer parameters characteristic of $\{FeNO\}(S = {}^3/_2)$.[30,84] In particular, we expect the strong delocalization produced by the overlap of Fe(d_{xz}) and Fe(d_{yz}) with NO π^* orbitals to be a general characteristic of these complexes. Consequently, our basic description of the electronic configurations of the iron and nitric oxide components of the $\{FeNO\}^7$ unit should also apply in those cases.

A motivation for the study of nitrosyl derivatives of hemerythrin has been their suggested role as analogues of a proposed superoxide intermediate in the dioxygen binding reaction. Strong experimental evidence for a mechanism that includes the superoxide intermediate is not available,[4] but Raman studies on deoxyHrNO which show hydrogen bonding to NO are consistent with such mechanism.[28] The additional valence electron of a superoxide intermediate would lead to a $\{FeOO\}^8$ unit. Previous calculations have shown that the occupied spin-down (β) orbitals with substantial OO(π^*) character in $\{FeOO\}^8$ contain less metallic contribution than their counterparts in $\{FeNO\}^7$.[34] This suggests that the effects of valence delocalization may be less significant in $\{FeOO\}^8$ complexes.[32]

7. Conclusion

We have performed a thorough analysis of Mössbauer spectra of the nitrosyl adducts of deoxyHr. High temperature spectra provided unique information about the isomer shifts, electric field gradients, and quadrupole splittings of the Fe^{2+} and $\{FeNO\}^7$ sites of deoxyHrNO and deoxyHrFNO. In addition, 4.2 K spectra recorded in applied fields allowed us to obtain a detailed characterization of the magnetic hyperfine interactions, zero-field splittings, and exchange interaction of deoxyHrNO.

To further understand the physical origin of Mössbauer parameters from $\{FeNO\}^7(S = {}^3/_2)$ sites we applied nonlocal gradient-corrected density functional theory to the representative complex $FeL(NO)(N_3)_2$. The self-consistent field calculations produced a detailed picture of the $S = {}^3/_2$ (ground state) Kohn−Sham wavefunction and the composition of key molecular orbitals which provide unique insight about the Fe−NO bond. Further analysis of the $S = {}^3/_2$ wavefunction yielded atomic charges, spin densities and NAO occupancies which allow comparison of $\{FeNO\}^7$ sites with other iron species and help to rationalize spin Hamiltonian parameters. We now summarize some of our results and conclusions:

(i) Mössbauer spectra of deoxyHrNO and deoxyHrFNO yielded isomer shifts and quadrupole splittings which clearly show the presence of two distinct iron species with intrinsic spin $S_1 = 2$ and $S_2 = {}^3/_2$, consistent with the high-spin ferrous and quartet-state $\{FeNO\}^7$ electronic configurations, respectively. Low-temperature applied field spectra of deoxyHrNO and deoxyHrFNO[76] are fully consistent with a Kramers doublet ground state that arises from antiferromagnetic coupling between its two iron species.

(ii) We have calculated Mössbauer spectra in the intrinsic spin representation from diagonalization of a $(2S_1 + 1) \times (2S_2 + 1) = 20$ Hamiltonian matrix. We have determined the Heisenberg exchange constant, zero-field splittings; *g* values, quadrupole splittings, and magnetic hyperfine tensors of Fe^{2+} and $\{FeNO\}^7$. The intrinsic parameters reported in Table 4 reproduce simultaneously Mössbauer spectra and g^{eff} from EPR.

(102) Gaussian 98, Revision A.1, Frisch, M. J.; Trucks, G. W.; Schlegel, H. B.; Scuseria, M. A.; Robb, M. A.; Cheeseman, J. R.; Zakrzewski, V. G.; Montgomery, J. A., Jr.; Stratmann, R. E.; Burant, J. C.; Dapprich, S.; Millam, J. M.; Daniels, A. D.; Kudin, K. N.; Strain, M. C.; Farkas, O.; Tomasi, J.; Barone, V.; Cossi, M.; Cammi, R.; Mennucci, B.; Pomelli, C.; Adamo, C.; Clifford, S.; Ochterski, J.; Petersson, G. A.; Ayala, P. Y.; Cui, Q.; Morokuma, K.; Malick, D. K.; Rabuck, A. D.; Raghavachari, K.; Foresman, J. B.; Cioslowski, J.; Ortiz, J. V.; Stefanov, B. B.; Liu, G.; Liashenko, A.; Piskorz, P.; Komaromi, I.; Gomperts, R.; Martin, R. L.; Fox, D. J.; Keith, T.; Al-Laham, M. A.; Peng, C. Y.; Nanayakkaara, A.; Gonzalez, C.; Challacombe, M.; Gill, P. M. W.; Johnson, B.; Chen, W.; Wong, M. W.; Andres, J. L.; Gonzalez, C.; Head-Gordon, M.; Replogle, E. S.; Pople, J. A. Gaussian, Inc.: Pittsburgh, PA, 1998.

(103) Barone, V. *Chem. Phys. Lett*. **1996**, *262*, 201.

(104) Rega, N.; Cossi, M.; Barone, V. *J. Chem. Phys*. **1996**, *105*, 11060.

(105) The isotropic Fermi contact and traceless tensor calculated at the U-B3PW91/6-311+G* level are $a_{iso} = -28.7$ MHz and $\tilde{a}_{dip} = (+9.6, +4.5, -14.1)$ MHz.

(106) Twilfer, H.; Bernhardt, F. H.; Gersonde, K. *Eur. J. Biochem*. **1985**, *147*, 171.

(iii) The nitrosyl adducts of deoxyHr correspond to a class of weakly coupled complexes where the condition $|J/D_i| \gtrsim 1$ applies. The ZFS strongly perturbs the eigenstates of the exchange interaction and mixes higher lying states with the doublet ground state.

(iv) We have also simulated Mössbauer 4.2 K spectra in the $S^{\text{eff}} = {}^1/_2$ representation which provides a useful link between Mössbauer data and EPR/ENDOR observables.

(v) Mössbauer parameters are consistent with bonding of NO to only one iron site of deoxyHr. The results are consistent with NO binding to the five-coordinate iron site that normally binds O_2 according to Scheme 1.

(vi) The drastic change in electronic configuration and, consequently, on Mössbauer parameters of one iron of deoxyHr upon binding to NO is consistent with reports[107−109] that Fe−NO bonding dominates the electronic structure of six-coordinate complexes containing an iron−nitrosyl group.

(vii) The isomer shifts of $\{FeNO\}^7(S = {}^3/_2)$ sites are larger than those expected for $Fe^{3+}(S = {}^5/_2)$ or $Fe^{3+}(S = {}^3/_2)$, and smaller than those expected for $Fe^{2+}(S = 2)$. Thus, irons within $\{FeNO\}^7$ groups can not be properly classified according to either of these configurations.

(viii) The spin-unrestricted $S = {}^3/_2$ Kohn−Sham wavefunction of the representative complex $FeL(NO)(N_3)_2$ contains molecular orbitals that strongly mix NO π^* with iron (d_{xz} and d_{yz}) orbitals. The corresponding delocalization produces a unique electronic configuration whereby some β electrons are almost equally shared by NO and the metal. We expect such strong mixing of NO π^* and metal orbitals to be a general characteristic of $\{FeNO\}^7(S = {}^3/_2)$ complexes.

(ix) The delocalization of some valence electrons within the $\{FeNO\}^7$ unit precludes the $FeL(NO)(N_3)_2$ complex from achieving full spin polarization. Since MOs 86β and 87β are distributed throughout NO, iron and the N_3 ligands, their individual NO π^* orbitals do not host nearly localized electrons or nearly whole units of β spin. Instead, the mixing with metal orbitals precludes the complex from achieving full spin polarization since some α and β electrons have, to some extent, a common spatial localization.

(x) The net α and β densities of iron and NO in $FeL(NO)(N_3)_2$ arise from the combined partial (i.e., not nearly whole) units of spin corresponding to some individual molecular orbitals with strong metal−ligand mixing. Such mixing does not allow for full spin polarization.

(xi) While the $Fe^{3+}(S = {}^5/_2)$ configuration typically gives rise to almost negligible zero field splittings (e.g., $|D| \gtrsim 0$), the corresponding parameters for spin coupled (Table 4) or uncoupled[35] $\{FeNO\}^7(S = {}^3/_2)$ sites are significantly larger (e.g., $D = 12-19$ cm^{-1}).

(xii) We conclude that neither of the idealized electronic configurations accurately represent the electronic configuration of iron or NO in $\{FeNO\}^7(S = {}^3/_2)$ species. We propose that it is more appropriate to regard iron and NO as integral parts of the $\{FeNO\}^7$ unit where some valence electrons are shared to a large extent by the entire moiety.

Acknowledgment. We thank D. M. Kurtz and J. M. Noceck who provided the samples used in Mössbauer experiments. The computational work was made possible by allocation grants from Mahui High Performance Computing Center (MHPCC), the Research Computing Cluster (RCC) of the University of Illinois, and the National Center for Supercomputer Applications (NCSA).

Supporting Information Available: Table of expectation values of operators ${}^1/_{14}\langle L_i^2 - 2\rangle$ (PDF). This material is available free of charge via the Internet at http://pubs.acs.org.

JA990129C

(107) Enemark, J. H.; Feltham, R. D.; Huie, B. T.; Johnson, P. L.; Swedo, K. K. *J. Am. Chem. Soc.* **1977**, *99*, 3285.
(108) Ballhausen, C. J.; Gray, H. B. *Inorg. Chem.* **1963**, *2*, 246.
(109) Manoharan, P. T.; Gray, H. B. *J. Am. Chem. Soc.* **1965**, *87*, 3340.
(110) Dawson, J.; Gray, H.; Hoenig, H. E.; Rossman, G.; Shredder, J.; Wang, R.-H. *Biochemistry* **1972**, *11*, 461.